Alma Mater Studiorum · Università di Bologna

Dipartimento di Fisica e Astronomia “Augusto Righi”
Corso di Laurea in Fisica

From White Dwarfs to Black Holes: A Computational Study of the Mass-Radius Relation

Relatrice:
Prof.ssa Barbara Lanzoni

Presentata da:
Zanko Ventsislavov Mezdrichki

Anno Accademico 2025/2026

Sommario

Gli oggetti compatti costituiscono laboratori ideali per testare teorie fisiche della materia in condizioni estreme. L'obiettivo di questa tesi è analizzare la relazione massa-raggio per nane bianche, stelle di neutroni e buchi neri (i cosidetti "oggetti compatti"), integrando la trattazione teorica con un'analisi computazionale. Le relazioni sono state ricavate risolvendo numericamente le equazioni differenziali di Lane-Emden e di Tolman-Oppenheimer-Volkoff tramite script Python, e vengono poi confrontate con dati osservativi al fine di discuterne i limiti di validità.

Vengono introdotti i fondamenti della fisica del gas degenere e i processi di evoluzione stellare che portano alla formazione degli oggetti compatti. Successivamente, l'analisi si concentra sulle nane bianche: viene ricavato computazionalmente il limite di Chandrasekhar, che fissa il valore massimo per la massa di strutture stellari mantenute in equilibrio idrostatico dalla pressione del gas degenere di elettroni, e si evidenziano le discrepanze tra il modello politropico non relativistico e le reali misurazioni astrofisiche. Per le stelle di neutroni, lo studio mette a confronto tre approcci diversi: si evidenziano i limiti dell'approssimazione Newtoniana e del modello ideale relativistico (TOV storico), mostrando come l'inclusione della forza nucleare forte tramite l'equazione di stato SLy4 sia necessaria per giustificare l'esistenza delle pulsar massicce osservate. Infine, lo studio si conclude con i buchi neri, analizzati attraverso la metrica di Schwarzschild, discutendo la natura dell'orizzonte degli eventi e della singolarità centrale.

Abstract

Compact objects constitute ideal laboratories for testing physical theories of matter under extreme conditions. The objective of this thesis is to analyze the mass-radius relation for white dwarfs, neutron stars, and black holes (collectively known as "compact objects"), combining theoretical treatment with computational analysis. These relations were derived by numerically solving the Lane-Emden and Tolman-Oppenheimer-Volkoff differential equations in Python, and are subsequently compared with observational data to discuss their limits of validity.

First, the foundations of degenerate gas physics and the stellar evolution processes leading to the formation of compact objects are introduced. Subsequently, the analysis focuses on white dwarfs: the Chandrasekhar limit, which determines the maximum mass of a stellar structure maintained in hydrostatic equilibrium by degenerate electron gas pressure, is derived computationally. Furthermore, discrepancies between the non-relativistic polytropic model and actual astrophysical measurements are highlighted. For neutron stars, the study compares three different approaches. The limitations of the Newtonian approximation and the ideal relativistic model (the original TOV model) are highlighted, demonstrating how the inclusion of the strong nuclear force via the SLy4 equation of state is necessary to account for the existence of observed massive pulsars. Finally, the study concludes with an analysis of black holes using the Schwarzschild metric, discussing the nature of the event horizon and the central singularity.

Contents

Introduction

The study of compact objects is fundamental to modern astrophysics, as these are natural laboratories for testing the validity of physical laws under conditions of extreme density and gravity. The fundamental parameter for understanding the internal structure and nature of these bodies is the mass-radius relationship, which reflects the equation of state of the matter composing the stellar core.

The central objective of this work is to analyze this relationship through a theoretical approach coupled with a computational analysis. The use of Python scripts developed for this study allowed me to numerically solve the differential equations of stellar structure, such as the Lane-Emden equation for polytropic regimes and the relativistic Tolman-Oppenheimer-Volkoff (TOV) equation. This methodology made it possible to explore the transition between different degeneracy regimes and to evaluate the impact of relativistic and nuclear corrections on the stability of compact objects.

To build this analysis, first the properties of degenerate matter are introduced. These are followed by a short description of the main phases of stellar evolution to understand the formation of compact objects. The computational methodology is then applied to white dwarfs, deriving the Chandrasekhar limit for their mass and comparing theoretical models with recent observational data from eclipsing binary systems. The focus then shifts to neutron stars, where the failure of the Newtonian approach is demonstrated, highlighting how General Relativity and the introduction of the repulsive strong nuclear force are necessary to account for the existence of massive pulsars. Finally, the investigation ends with Schwarzschild black holes, where gravity overcomes all quantum degeneracy pressures, leading to an inevitable collapse.

Chapter 1

Physics of Degenerate Matter

To understand the birth of compact objects, in particular white dwarfs and neutron stars, a detailed description of the principles of quantum mechanics that allow their existence is necessary. In this chapter, the properties of degenerate matter will be discussed in detail.

1.1 Transition from ideal gas to degenerate gas

To understand the transition from ideal to degenerate gas, it is crucial to determine when quantum effects can no longer be neglected. Since neutrons and electrons are fermions, that is, particles with spin $s = \frac{1}{2}$, they follow Fermi-Dirac statistics. These particles must comply with Heisenberg's uncertainty principle, which states that it is impossible to specify simultaneously, with arbitrary precision, both the momentum and the position of a particle. If the uncertainty in the measurement of the position is Δx and the uncertainty in the momentum is Δp_x, then the product of the two uncertainties can never be less than $\hbar/2$, where $\hbar$ is the reduced Planck constant. The other principle they must respect is the Pauli exclusion principle, according to which in a system of fermions, it is impossible for two particles to have all the same quantum numbers, that is, to occupy the same state.

All this has dramatic consequences on the behavior of degenerate matter, which deviates completely from an ideal gas. In fact, due to these two principles, it is shown that at temperature $T = 0$ the total energy of the gas can be non-zero, depending on the total number of particles. Such energy, which is the maximum possessed by a particle of the gas of fermions at a fixed number of particles, is called Fermi energy. Calculating this energy is necessary to define the criterion for which quantum effects become dominant.

By solving the stationary Schrödinger equation for a 3-D potential well, one obtains the different possible energy values that an electron can take. The result is as follows

$$E = \frac{\hbar^2 \pi^2}{2 m_e V^{\frac{2}{3}}} (n_x^2 + n_y^2 + n_z^2), \tag{1.1}$$

with m_e being the mass of the electrons, V the total volume, n_x, n_y, n_z positive integers each representing a specific microstate of the system with energy E. It is worth noting the quantization of energy, a concept introduced by quantum mechanics.

To calculate the number of possible states, it is convenient to move to phase space. The formula to use, assuming that the system is the same in all directions, thus obtaining spherical symmetry, is the following:

$$dN = g_s 4\pi k^2 dk \frac{V}{(2\pi)^3}. \tag{1.2}$$

The term in the right-hand of the equation represents the "infinitesimal cube" of volume in k-space occupied by each state. The factor g_s was introduced to take into account the spin degeneration (usually it is 2).

It is useful to introduce the concept of density of states (number of states per unit energy) given by:

$$g(E) = \frac{dN}{dE}. \tag{1.3}$$

In the case of a particle confined in a 3-D potential well, the kinetic energy E of each particle is related to the magnitude of its wave vector k by the standard dispersion relation:

$$E = \frac{\hbar^2 k^2}{2m_e}. \tag{1.4}$$

Using this relation, the density of states as a function of energy becomes:

$$g(E) = \frac{g_s}{4\pi^2}\left(\frac{2m_e}{\hbar^2}\right)^{\frac{3}{2}} V E^{\frac{1}{2}}. \tag{1.5}$$

At this point it is possible to calculate the chemical potential μ, assuming a fixed number of particles, using the equation:

$$N = \int_0^\infty g(E) f(E) dE \tag{1.6}$$

and the expression of the Fermi-Dirac distribution

$$f(E) = \frac{1}{e^{\frac{\epsilon-\mu}{k_b T}} + 1}. \tag{1.7}$$

The chemical potential μ is an intensive thermodynamic quantity that expresses the change in the free energy of a system as a function of the number of particles added or removed, keeping the other state variables constant.

To obtain the criterion for which quantum effects become dominant, we are interested in the case where $T = 0$ and in this situation we can approximate the Fermi-Dirac distribution with the Heaviside step function at $\epsilon = \mu$.

Using the equation (1.6), we obtain N as a function of μ, and isolating the latter we obtain the following result:

$$\mu(T=0) = \epsilon_F = \frac{\hbar^2}{2m_e}\left(\frac{6\pi^2 n}{g_s}\right)^{\frac{2}{3}}, \tag{1.8}$$

with $n = N/V$. The expression in equation (1.8) is the Fermi energy. It separates occupied states from unoccupied ones. For a gas of electrons (spin 1/2 fermions),

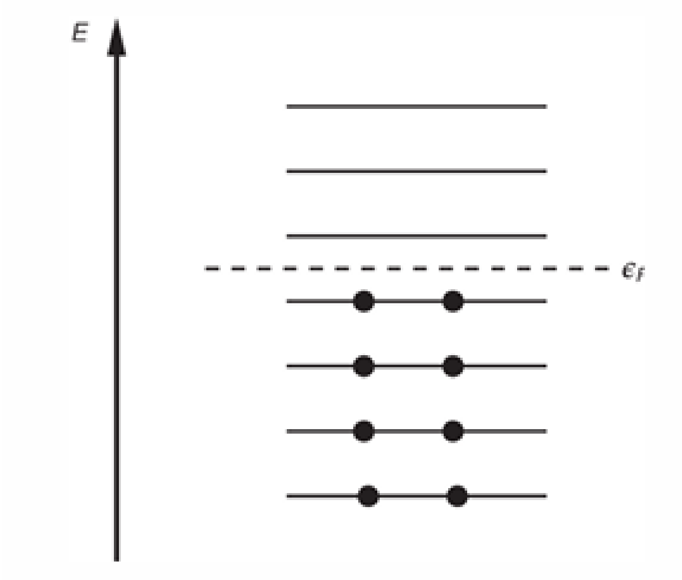

Figure 1.1: Diagram showing how electrons occupy energy levels below the Fermi energy, which separates the occupied levels from the empty ones. Image adapted from [1].

at $T = 0$ every level below ϵ_f is doubly occupied. The Fermi energy is nothing more than the maximum energy that a particle can assume. Figure (1.1) shows a visualization of this concept.

This allows for the definition of the criterion that separates the classical ideal gas from the degenerate regime.

Quantum effects become relevant when the thermal energy of the particles is less than the Fermi energy. The mathematical condition is:

$$k_bT \ll \epsilon_F. \tag{1.9}$$

By isolating the temperature T, the criterion is:

$$T \ll \frac{\hbar^2(3\pi^2 n)^{\frac{2}{3}}}{2m_e k_b}. \tag{1.10}$$

It is more useful to express the result just obtained as a function of mass density (ρ). Substituting

$$n = \frac{\rho}{\mu_e m_H}, \tag{1.11}$$

where m_H is the mass of hydrogen, and μ_e is the mean molecular weight of an electron gas. Such a change leads to:

$$\frac{T}{\rho^{\frac{2}{3}}} \ll \frac{\hbar^2}{2mk_b}\left(\frac{3\pi^2}{\mu_e m_H}\right)^{\frac{2}{3}}. \tag{1.12}$$

This inequality shows that the higher the density, the less negligible the quantum effects are. Since the density in white dwarfs is extreme (on the order of 10^6 g cm^{-3}), the temperature on the left can reach values of $\approx 10^9$ K. This means that even if the interior of the white dwarf is very hot (e.g. $10^7 K$), the inequality is largely satisfied and the electrons are degenerate.

This criterion in eq. (1.10) was derived by neglecting the effects of special relativity. In the case in which the density n increases, the velocities of the individual particles begin to approach the speed of light c. In that case, it is necessary to use another formula for energy. This changes the values of the density of states, and consequently of all the quantities that depend on it.

1.2 Degenerate gas pressure

Once the conditions for degeneracy are established, it is necessary to analyze the macroscopic properties of degenerate matter and its role in compact objects. Since one of the assumptions in the stellar model is that the star is in hydrostatic equilibrium, it is necessary to describe the pressure exerted by a degenerate gas.

The pressure of a system with an isotropic distribution of momenta is given by:

$$\frac{1}{3}\int pvn(p)dp, \tag{1.13}$$

where v is the velocity, p the momentum and n the number density of particles. Recalling eq. (1.2) and using the well-known relationship between momentum and wave vector($p = \hbar k$), it is possible to write n as a function of p:

$$n(p)dp = \frac{8\pi}{h^3}p^2 dp. \tag{1.14}$$

Since the energy has a maximum, that is, the Fermi energy, the momentum should also not be integrated up to infinity, but up to the Fermi momentum, which is:

$$p_F = \sqrt[3]{\frac{3h^3}{8\pi\mu_e m_H}}\rho^{\frac{1}{3}}. \tag{1.15}$$

This value was obtained by integrating eq.(1.14) from 0 to p_0 and using relation (1.11).

To solve the integral in eq. (1.13) analytically, it is convenient to define a dimensionless Fermi momentum, by

$$x = \frac{p_F}{m_e c}. \tag{1.16}$$

This parameter can also be expressed as a function of the mass density:

$$x = 1.0088 \times 10^{-2}(\frac{\rho}{\mu_e})^{\frac{1}{3}}. \tag{1.17}$$

The pressure is given by eq.(1.13), and writing the speed v as $v = pc^2/E$, where

$E = \sqrt{m_e^2c^4 + p^2c^2}$:

$$\begin{aligned} P_e &= \frac{1}{3}\frac{8\pi}{h^3}\int_0^{p_F} \frac{p^2c^2}{\sqrt{m_e^2c^4+p^2c^2}}p^2dp \\ &= \frac{8\pi m_e^4c^5}{3h^3}\int_0^x \frac{y^4}{\sqrt{(1+y^2)}}dy \\ &= \frac{m_ec^2}{\lambda_e^3}\phi(x) \\ &= 1.42180\times 10^{25}\phi(x)\ \ \text{dyne}\,\text{cm}^{-2}, \end{aligned} \tag{1.18}$$

where $\phi(x)$ is a function of x and $\lambda_e = \frac{\hbar}{m_ec}$ is the electron Compton wavelength.

It is possible to show that in the limit where $x \ll 1$ (non-relativistic electrons), $\phi(x)$ can be approximated to first order as $\phi(x) = \frac{x^5}{15\pi^2}$, while for $x \gg 1$ (relativistic electrons) $\phi(x) = \frac{x^4}{12\pi^2}$.

The equation of state can be written in the polytropic form:

$$P = K\rho^\Gamma, \tag{1.19}$$

where K and Γ are constants.

For non-relativistic electrons, so when $\rho \ll 10^6$ g cm^{-3} and $x \ll 1$:

$$\begin{aligned} \Gamma_1 &= \frac{5}{3} \\ K_1 &= \frac{3^{2/3}\pi^{4/3}}{5}\frac{\hbar^2}{m_em_H^{5/3}\mu_e^{5/3}} = \frac{1.0036\times 10^{13}}{\mu_e^{5/3}}\text{cgs}. \end{aligned} \tag{1.20}$$

For relativistic electrons, so when $\rho \gg 10^6$ g cm^{-3} and $x \gg 1$:

$$\begin{aligned} \Gamma_2 &= \frac{4}{3} \\ K_2 &= \frac{3^{1/3}\pi^{2/3}}{4}\frac{\hbar c}{m_H^{4/3}\mu_e^{4/3}} = \frac{1.2435\times 10^{15}}{\mu_e^{4/3}}\text{cgs}. \end{aligned} \tag{1.21}$$

These results apply to a degenerate electron gas, but it is possible to derive these formulas also for a neutron gas.

For non-relativistic neutrons, so when $\rho \ll 10^{15}$ g cm^{-3}:

$$\begin{aligned} \Gamma_1 &= \frac{5}{3} \\ K_1' &= \frac{3^{2/3}\pi^{4/3}}{5}\frac{\hbar^2}{m_n^{8/3}} = 5.3802\times 10^9 cgs. \end{aligned} \tag{1.22}$$

For relativistic neutrons, so when $\rho \gg 10^{15}$ g cm^{-3}:

$$\begin{aligned} \Gamma_2 &= \frac{4}{3} \\ K_2' &= \frac{3^{1/3}\pi^{2/3}}{4}\frac{\hbar c}{m_n^{4/3}} = 1.2293\times 10^{15}\text{cgs}. \end{aligned} \tag{1.23}$$

These results will be used in Chapters 3 and 4, where they will be applied to white dwarfs and neutron stars.

Chapter 2

Stellar Evolution

Before analyzing compact objects, it is necessary to understand how they form. To this end, the present this chapter will discuss the main phases of stellar evolution.

2.1 Star formation

Stars form from the contraction of gas clouds. For a cloud to be in stable equilibrium, the total kinetic energy (K) and the gravitational potential energy (U) must satisfy the so-called Virial Theorem:

$$2K + U = 0. \tag{2.1}$$

Collapse occurs when gravity overcomes the internal pressure; that is, when:

$$|U| > 2K \tag{2.2}$$

Assuming a spherical cloud of mass M, radius R, uniform density ρ and temperature T, it can be shown that the potential energy of the cloud is:

$$U = -\frac{3}{5}\frac{GM^2}{R}, \tag{2.3}$$

where G is the gravitational constant.

Kinetic energy is the sum of the thermal energies of the particles that make up the cloud:

$$K = \frac{3}{2}Nk_bT = \frac{3}{2}\frac{M}{\mu m_H}k_bT. \tag{2.4}$$

Here k_b is the Boltzmann constant, and the number of particles (N) has been calculated as the ratio of the total mass (M) to the mean molecular weight (μ) multiplied by the mass of hydrogen (m_H), assuming that the cloud is composed predominantly of this element. By imposing the instability condition of eq. (2.2), the following inequality is obtained:

$$\frac{3}{5}\frac{GM^2}{R} > 3\frac{M}{\mu m_H}k_bT. \tag{2.5}$$

Simplifying and isolating M, and remembering that for a sphere of mass M and radius R, the density is $\rho = M/(4/3\pi R^3)$, the critical mass (the so-called Jeans mass M_J) above which the gas cloud collapses is obtained:

$$M_J = \left(\frac{5k_b}{Gm_H\mu}\right)^{\frac{3}{2}} T^{\frac{3}{2}}\rho^{-\frac{1}{2}}. \tag{2.6}$$

This shows that dense and cold clouds offer the needed conditions for star formation to occur. The Jeans approach is simple, as it neglects effects such as turbulence in the medium and magnetic fields, but it is effective in identifying the ideal environmental conditions that favor star formation. However, the mechanisms that trigger the collapse of gas clouds are still debated.

The contraction process favors the formation of stellar aggregates, with fragmentation processes of the collapsing cloud being responsible for the formation of stars of different masses.

There are mass limits for the formation of stars:

For $M > 100\mathrm{M}_\odot$ the stellar structure becomes unstable. This is not a rigorous cut-off (it mainly depends on metallicity), but it is difficult to form such massive stable stars because their luminosity tends to overcome the Eddington limit, making radiation pressure much higher than gravity.

For $M < 0.08\ \mathrm{M}_\odot$ the central temperature is too low to ignite hydrogen fusion. Such objects are called brown dwarfs.

The contraction of each fragment (proto-star) of suitable mass continues until core temperatures are high enough ($T \sim 10^7$ K) to ignite hydrogen fusion, entering the Main Sequence, and transforming the proto-star into a star.

2.2 Hertzsprung–Russell diagram

The Hertzsprung–Russell diagram (H–R diagram) is a plot showing the relationship between luminosity and the effective temperature of stars of different masses during their lifetimes, i.e., the so-called "stellar evolutionary tracks" (see Figure 2.1, where each line is labeled with the value of the corresponding stellar mass in units of the solar mass, ranging from 30 $\mathrm{M}_\odot$ at the top-left corner, to 0.5 $\mathrm{M}_\odot$ at the bottom-right end). The diagram represented is a very useful tool to summarize the main steps of stellar evolution.

The diagram plots star's luminosity (L) normlized to the luminosity of the Sun on the ordinate against its effective surface temperature (T_{eff}) in Kelvin degree on the abscissa, with the convention that temperature increases toward the left.

In addition, it also traces the time variation of the physical size (radius) of each stars. This is because stellar emission is very well approximated by the black-body radiation, which follows the Stefan-Boltzman law:

$$L = 4\pi R^2 \sigma T_{eff}^4, \tag{2.7}$$

where σ denotes the Stefan-Boltzmann constant and R is the stellar radius. By rearranging eq. 2.7, R can be expressed as:

$$R = \sqrt{\frac{L}{4\pi\sigma T_{eff}^4}}. \tag{2.8}$$

In logarithmic terms, eq. 2.8 implies that lines of constant radius are oblique in the graph with a negative slope, as indicated by the "constant R" line shown in Figure 2.1.

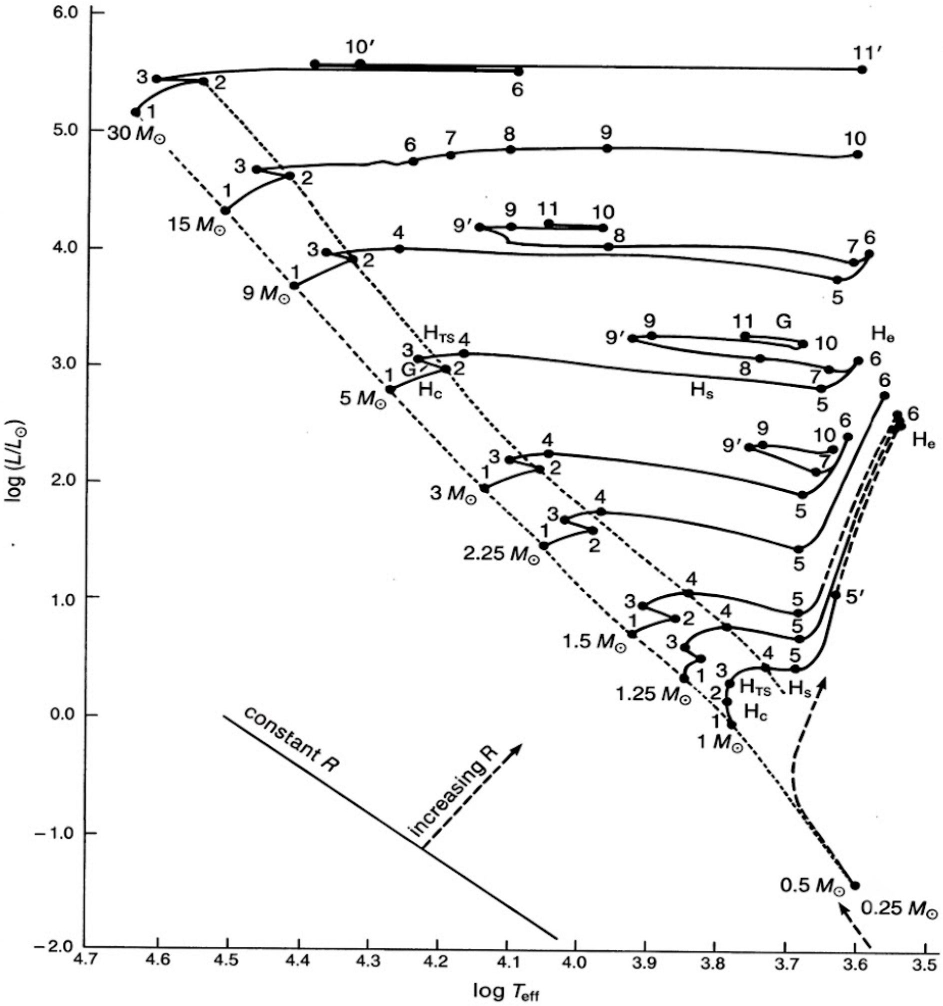

Figure 2.1: H–R diagram illustrating evolutionary tracks for stars from $0.5\,M_\odot$ to $30\,M_\odot$. The luminosity in logarithmic solar units $\log(L/L_\odot)$ is shown on the Y-axis, while the horizontal axis displays $\log T_{\rm eff}$ increasing toward the left. The dashed lines highlight the main sequence (MS) boundaries, from the Zero-Age Main Sequence (ZAMS, the rightmost dashed line) to the end of the MS. A visual reference for lines of constant radius and the direction of increasing radius are also depicted. The dots and numbers labeled along each track represent different stages of the star's evolution. Image adapted from[2].

The dotted line connecting the points labeled 1 along the various tracks in Figure 2.1 defines the ZAMS (Zero-Age Main Sequence): the sequence in the HR diagram where stars of different masses are located at the moment of H-burning ignition in their core.

The Main Sequence phase, representing the evolution from the ZAMS to the exhaustion of core hydrogen burning, corresponds to segment 1-2 along each track.

Segments 3-4-5 describe the Subgiant Branch (SGB) for low-mass stars or the Hertzsprung gap for high-mass stars, while segment 5-6 represents the Red Giant Branch (RGB).

The remaining points illustrate the final stages leading to stellar death, where the evolutionary tracks take completely different paths depending on the initial mass of the star.

All these different stages will be described in more detail in the following sections.

2.3 The Main Sequence

When the stellar core reaches 10 million Kelvin degrees, hydrogen burning thermonuclear reactions begin. This phase is called "main-sequence" (MS). For stars with a mass up to $\sim 1.2\ M_{\odot}$, the dominant hydrogen-burning process is the so called "proton-proton (or p-p) chain". Figure 2.2 shows the nuclear reactions that characterize this chain. Hydrogen fuses first into deuterium and then into helium.

In stars of slightly over 1.2 $M_{\odot}$, where the core can reach a temperature of 1.8×10^7 K, the carbon–nitrogen–oxygen fusion reaction (CNO cycle), represented in Figure 2.3, contributes a large portion of the energy generation.

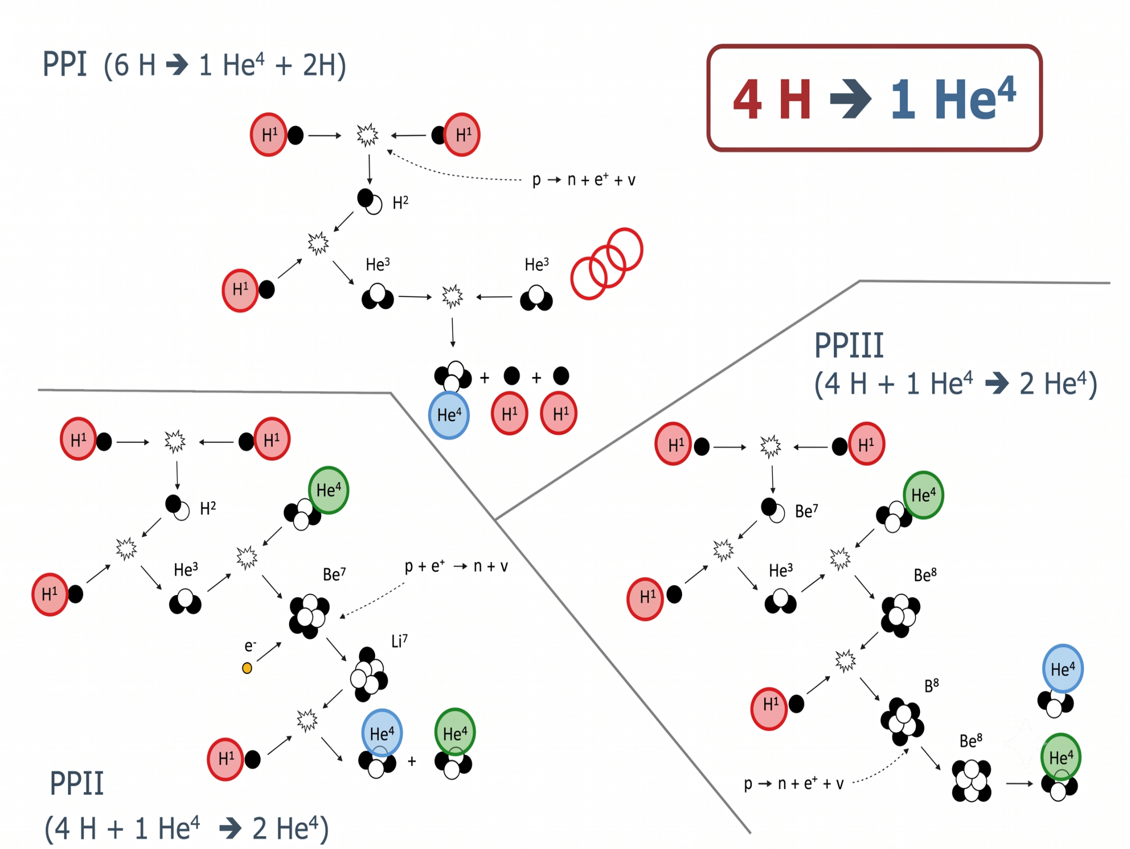

Figure 2.2: The PP chain. Initially the PPI chain is dominant. Then, as the abundance of He^4 increases, the probability of the He^4 + He^3 reaction increases, leading to the rise of the PPII and PPIII chains. Image adapted from [2].

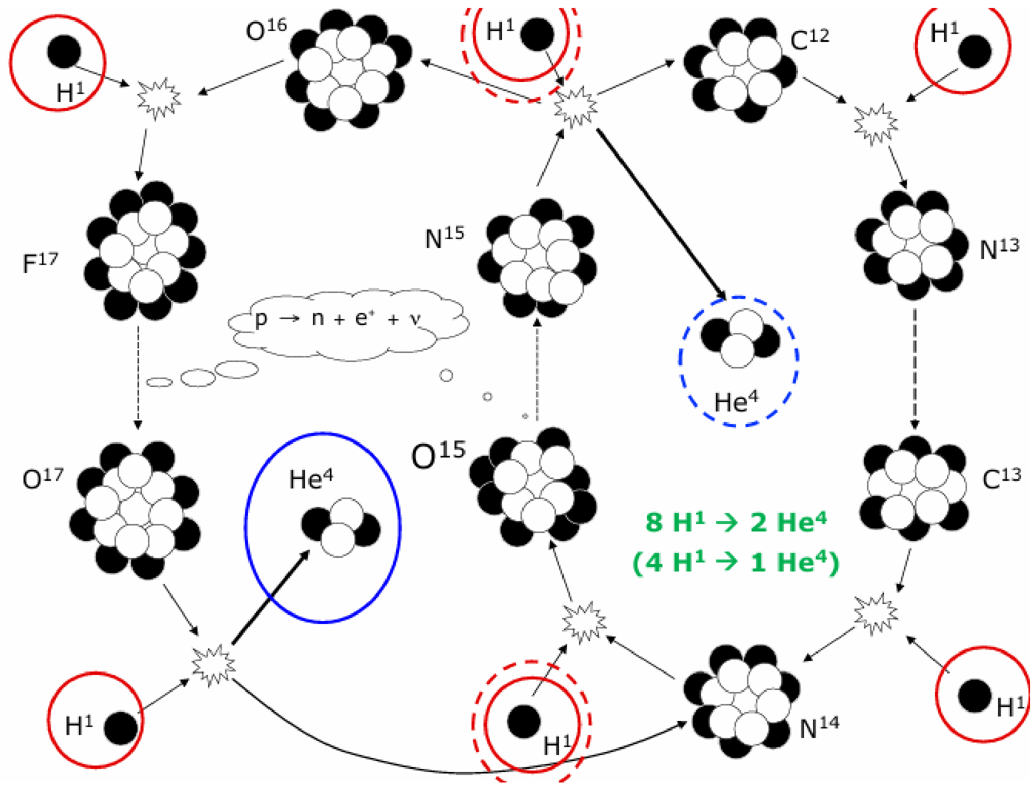

Figure 2.3: The CNO cycle. All the nuclear reactions that make up the cycle are highlighted. Also in this case, the chain tranforms 4 protons into a nucleus of He^4, while C, O, and N acts as nucler catalysts. Image adapted from [2].

The onset of nuclear fusion rapidly establishes hydrostatic equilibrium. The energy released by the core generates a strong outward thermal pressure, which balances the gravitational weight of the star and prevents further collapse. During the MS phase, the macroscopic characteristics of stars, such as luminosity (L), effective temperature (T_{eff}), and radius (R), change very little. The MS is by far the longest evolutionary stage in star's lifetime. This is because the H-burning process is the most efficient thermonuclear reaction.

There is a very strong relationship between the star mass and the MS phase duration:

$$t_{ms} \approx 10^{10} \left(\frac{M}{M_\odot} \right)^{-2.5} \text{yr}. \tag{2.9}$$

Since the Big Bang happened $\sim$ 13.7 Gyr ago, all the stars with $M < 0.8\ \mathrm{M}_\odot$ that formed in the early Universe are still burning H in their cores.

2.4 Post-Main Sequence and Final Fates

The end of the main-sequence phase occurs when hydrogen burning ceases in the stellar core. The inert He core begins to contract under its own gravity, causing its central temperature and density to rise. This heats the surrounding layers, igniting hydrogen fusion in a shell around the core. The gravitational potential energy released by the contraction, combined with the energy from the shell burning, forces the stellar envelope to expand. Consequently, the effective temperature drops and the star undergoes a redward evolution on the Hertzsprung-Russell diagram, entering the Subgiant Branch (SGB).

As the core continues to contract, the temperature and density of the hydrogen-burning shell increase. Although the shell begins to narrow significantly, the energy generation rate of the shell increases rapidly. This enormous internal energy production leads to the expansion of the stellar envelope, moving the star up the Red Giant Branch (RGB). While R keeps increasing, T_{eff} cannot decrease much further because the star is approaching its Hayashi track (the limit for stable structures): T_{eff} decreases only mildly, and therefore L increases substantially, especially for low-mass stars that develop a degenerate core (see below). The RGB phase ends with the start of core Helium burning, which occurs through the so-called "3 α chain", where 3 α particles (He^4 nuclei) generate a nucleus of C^{12} (see Figure 2.4).

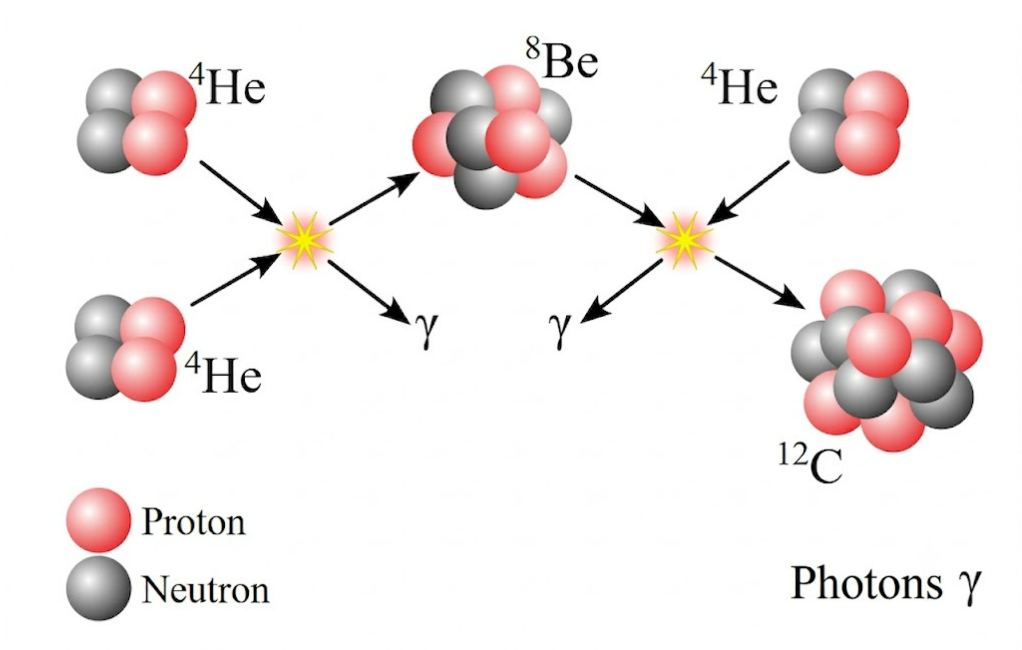

Figure 2.4: The Triple-Alpha chain. The nuclear fusion of two He^4 nuclei produces Be^8, which is highly unstable and decays back into two alpha particles, unless within that time a third alpha particle fuses with the Be^8 nucleus to produce a C^{12} nucleus. Image adapted from [3].

Stars with mass $M < 2.2$ M$_\odot$ develop a degenerate core during their RGB evolution. The electron-degeneracy contrasts the contraction of the core. The He-ignition is therefore delayed and occurs under critical semi-degenerate conditions, with a huge release of energy. This phenomenon is called He-flash.

2.4.1 Very Low-Mass Stars ($M < 0.5$ M$_\odot$)

Stars with an initial mass $M < 0.5$ M$_\odot$ cannot burn helium in their core because they are unable to reach the necessary ($\sim 10^8$K) internal temperatures. No other thermonuclear burning is allowed: they become He white dwarfs.

As said before, no stars with $M < 0.5\ \mathrm{M}_\odot$ have finished the core H-burning phase yet. Hence, not a single He-WD should exist in the Universe. However, many have been observed because they are the peeled cores of RGB stars that lost their envelope due to interaction with another star in a binary system.

2.4.2 Intermediate-Mass Stars ($0.5\ \mathrm{M}_\odot < M < 8\ \mathrm{M}_\odot$)

When central He-burning is exhausted (i.e., the so-called horizontal branch or red clump phase ends), core helium burning ceases and the core contracts. The internal density and temperature conditions cross the electron degeneracy limit again. An electron degenerate carbon-oxygen core develops, and central thermonuclear fusion permanently stops.

Hydrostatic equilibrium is temporarily maintained by helium burning in a surrounding shell (the early asymptotic giant branch -AGB- phase), and later by alternating hydrogen and helium shell burning (the thermal pulses AGB phase). The star's gravitational potential energy is insufficient to heat the core to the temperatures required for carbon ignition ($\approx 6 \times 10^8$ K).

Meanwhile, the stellar envelope expands. As the surface gravity decreases, the external regions become less bound and the star loses mass at an impressive rate through intense stellar winds. Eventually, the nuclear shells are extinguished, leading to the end of the AGB phase and the formation of a Planetary Nebula from the expelled envelope.

What remains is a C−O White Dwarf: a stellar corpse composed of electron degenerate matter that no longer undergoes nuclear fusion. The structural properties and the strict mass limits of these objects will be the core subject of Chapter 3.

2.4.3 Massive Stars ($M > 8\ \mathrm{M}_\odot$)

When central He-burning is exhausted, the core contracts. However, unlike in lower-mass stars, the gravity of these massive objects ensures that the core temperature increases enough to allow the sequential ignition of increasingly heavier elements in conditions of ideal, non-degenerate gas. As the core burning of a given element concludes, stable burning of the same element starts in a shell, creating an "onion-like" internal structure.

This thermonuclear sequence halts when the core is converted into iron (Fe). Since iron-peak elements possess the highest binding energy per nucleon, further fusion is endothermic. Lacking a central source of thermal energy, the inert Fe core contracts and becomes supported by electron degeneracy pressure.

As the central density increases, inverse beta decay becomes energetically favorable. Protons and electrons merge into neutrons, emitting a massive flux of neutrinos. This electron capture process reduces the number of free electrons, removing the primary source of degeneracy pressure that sustains the core against gravity. The simultaneous loss of energy through neutrinos accelerates the runaway collapse.

When the density approaches the nuclear saturation density ($\rho_{nuc} \approx 2.8 \times 10^{14}$ $\mathrm{g\,cm^{-3}}$), the inner portion of the collapsing core (≈ 0.7 $M_\odot$) comes to an abrupt halt, stabilized by neutron degeneracy pressure and the strong nuclear force. The outer layers, still in free fall, slam into this dense obstacle and bounce back, generating a powerful shockwave.

At these extreme densities, the material becomes opaque even to neutrinos. The trapped neutrinos deposit their immense thermal energy into the matter, supporting the propagating shockwave. The shockwave moves out through the star and produces a Core-Collapse (Type II) Supernova explosion.

The nature of the surviving remnant depends entirely on its final mass that, in turn, is determined by the initial stellar mass:

- If the remnant mass is below the modern relativistic TOV limit, it stabilizes as a Neutron Star (analyzed in Chapter 4). This is the fate of stars with an initial mass between ~ 8 $M_\odot$ and ~ 25 $M_\odot$.

- If the remnant mass exceeds this theoretical limit, gravity defeats all quantum mechanical forces, causing an unstoppable collapse into a Black Hole (discussed in Chapter 5). It's the end of the stars with $M_{in} > 25$ $M_\odot$.

Chapter 3

White Dwarfs

White dwarfs (WDs) represent the final evolutionary stage for small and medium-sized stars with initial masses up to approximately 8 $M_\odot$. Consequently, they are the end product of stellar evolution for 95-98% of all stars. They are compact objects of about one solar mass, with a typical radius of roughly 5000 km (approximately the Earth radius) and a mean density of the order of 10^6 g cm^{-3}.

Furthermore, due to the highly efficient conductive energy transport by degenerate electrons, white dwarfs are essentially isothermal structures. They maintain a nearly constant internal temperature of approximately 10^7 K from the center up to the outermost layers. At the surface, the temperature sharply drops to $\sim 10^4$ K across a thin, non-degenerate envelope primarily composed of hydrogen (and sometimes helium).

Since thermonuclear fusion has stopped, a white dwarf simply radiates its residual thermal energy into space, becoming cooler and less luminous over time. The rate at which it cools depends on its mass: more massive white dwarfs cool down more slowly. Mathematically, the cooling time t_{cool} required to reach a certain luminosity L can be approximated as $t_{cool} \propto M^{\frac{5}{7}} L^{-\frac{5}{7}}$, where M is the mass of the white dwarf.

When nuclear burning ceases, the outward thermal pressure drops, and the stellar core undergoes a gravitational contraction. This collapse is ultimately halted not by thermal gas pressure, but by the purely quantum mechanical effect of electron degeneracy pressure. Therefore, the very existence of WDs, the mass-radius relation, and the limiting Chandrasekhar mass (see below) are macroscopic demonstrations of the Heisenberg uncertainty principle and Pauli exclusion principle for fermions, topics extensively covered in Chapter 1.

WDs offer cosmic laboratories with extreme physical conditions that cannot be achieved in terrestrial facilities. A major advantage of WDs is that their surfaces can be observed directly and studied with the classical methods of spectroscopy and stellar atmosphere modeling. This provides reliable data for effective temperatures, surface gravities, element abundances, and parameters derived from these observations, such as masses, radii, and ages.

In this chapter, the theory behind the internal structure of these objects will be discussed by coupling the degenerate equation of state with the classical equations of hydrostatic equilibrium. Furthermore, a computational analysis of the mass-radius relationship will be carried out, and the numerical results will be compared with experimental observational data.

3.1 The Lane-Emden equation

To model the interior of a white dwarf, several physical assumptions are required. For a spherically symmetric distribution of matter, the mass is related to the radius by the following relationship:

$$\frac{dm}{dr}(r) = 4\pi r^2 \rho \tag{3.1}$$

In stellar models, it is assumed that the star is in a steady state. The force of gravity balances the pressure force at every point. To maintain this equilibrium, the net force on any volume element must be zero.

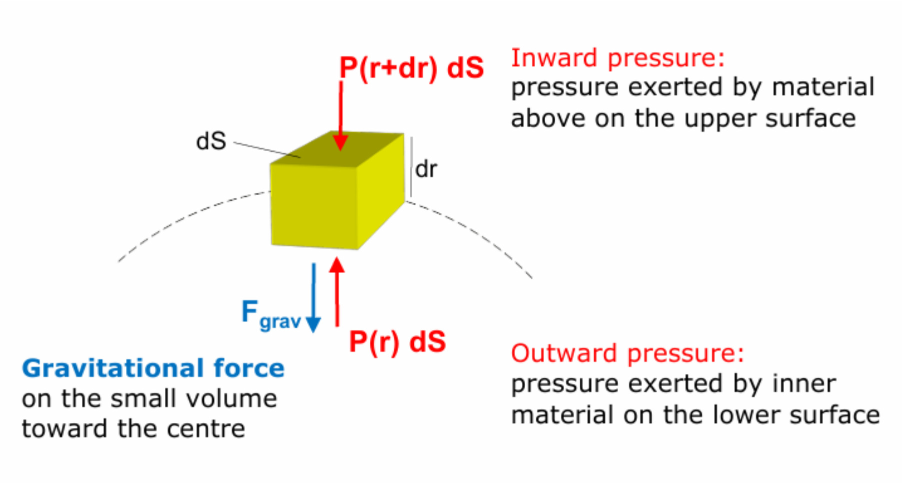

Figure 3.1: Forces acting on a cube of infinitesimal volume of mass dm. Image adapted from [2].

In Figure (3.1) all the acting forces are highlighted.
The pressure force is given by:

$$F_{press} = -[P(r + dr) - P(r)]dS. \tag{3.2}$$

This must balance the gravitational force:

$$F_{grav} = -\frac{GM(r)}{r^2}\rho(r)dSdr. \tag{3.3}$$

By setting the sum of these two forces equal to zero and taking the limit for $dr \to 0$, the standard equation for hydrostatic equilibrium is obtained:

$$\frac{dP}{dr} = -\frac{GM(r)}{r^2}\rho(r). \tag{3.4}$$

In general, hydrostatic equilibrium implies $\nabla P = -\rho \nabla \Phi$, where Φ is the gravitational potential.

These two classical equations can now be coupled with the polytropic equation of state derived in Chapter 2, eq. (1.19). As previously discussed, this equation assumes a fully degenerate electron gas, which is an excellent approximation since the internal temperature and density values of WDs largely satisfy the degeneracy criterion expressed in eq. (1.12). Together, these relations provide a closed system of three equations for three unknown variables: pressure P, density ρ, and enclosed mass $m(r)$.

The combination of eq.(3.1) and eq.(3.4) allows obtaining

$$\frac{1}{r^2}\frac{d}{dr}\left(\frac{r^2}{\rho}\frac{dP}{dr}\right) = -4\pi G\rho. \tag{3.5}$$

We can now substitute $P = K\rho^{\Gamma}$ and write

$$\Gamma \equiv 1 + \frac{1}{n}, \tag{3.6}$$

where n is called the polytropic index. For the solution of the differential equation, it is convenient to introduce the following dimensionless parameters:

$$\rho = \rho_c\theta^n, \tag{3.7}$$

$$r = a\xi, \tag{3.8}$$

$$a = \left[\frac{(n+1)K\rho_c^{(1/n-1)}}{4\pi G}\right]^{\frac{1}{2}}, \tag{3.9}$$

where $\rho_c = \rho(r=0)$ is the central density. In this way, the Lane-Emden equation for the structure of a polytrope of index n is obtained:

$$\frac{1}{\xi^2}\frac{d}{d\xi}\left(\xi^2\frac{d\theta}{d\xi}\right) = -\theta^n. \tag{3.10}$$

The boundary conditions at the center of a polytropic star are:

$$\theta(0) = 1, \tag{3.11}$$

$$\theta'(0) = 0. \tag{3.12}$$

The condition (3.11) follows from eq. (3.7). The other condition comes from the fact that $m(r) \approx \frac{4}{3}\pi\rho_c r^3$ near the center so that by eq. (3.4), $\frac{dP}{dr} = 0 = \frac{d\rho}{dr}$.

3.2 The M-R relation and the Chandrasekhar Limit

The Lane-Emden equation can be integrated numerically, as will be done in the following section, taking into account the boundary conditions. For $n < 5$, the solutions have a zero at a finite value $\xi = \xi_1$: $\theta(\xi_1) = 0$. This point corresponds to the surface of the star, so:

$$R = a\xi_1 = \left[\frac{(n+1)K}{4\pi G}\right]^{\frac{1}{2}} \rho_c^{\frac{1-n}{2n}}\xi_1 \tag{3.13}$$

As for the mass, starting from eq. (3.1) and using eq. (3.7) and eq. (3.10):

$$\begin{aligned}
M &= \int_0^R 4\pi r^2 \rho dr \\
&= 4\pi a^3 \rho_c \int_0^{\xi_1} \xi^2 \theta^n d\xi \\
&= -4\pi a^3 \rho_c \int_0^{\xi_1} \frac{d}{d\xi}(\xi^2 \frac{d\theta}{d\xi}) d\xi \\
&= 4\pi \left[\frac{(n+1)K}{4\pi G}\right]^{\frac{3}{2}} \rho_c^{\frac{3-n}{2n}} \xi_1^2 |\theta'(\xi_1)|. \qquad (3.14)
\end{aligned}$$

By isolating ρ_c from the equation for the radius and inserting it into the mass equation, the mass-radius relation for polytropes is obtained:

$$M = 4\pi R^{\frac{3-n}{1-n}} \left[\frac{(n+1)K}{4\pi G}\right]^{\frac{n}{n-1}} \xi_1^{\frac{3-n}{1-n}} \xi_1^2 |\theta'(\xi_1)|. \qquad (3.15)$$

It is interesting to analyze the solutions for $n = \frac{3}{2}$ and $n = 3$, which are the cases of non-relativistic and relativistic degenerate gas, discussed in Chapter 2, with eq. (1.20) and eq. (1.21).

It is worth noting that in the case of relativistic electrons, the exponent of R becomes zero, thus obtaining a limiting mass value, while for $n = 3/2$ a proportionality relation between mass and radius comes out from eq. (3.15):

$$M \propto R^{-3}. \qquad (3.16)$$

Substituting $n = 3$ into the mass equation, the total mass of the star becomes strictly independent of both its central density and its radius. This represents a critical physical threshold: the Chandrasekhar limit [4, 5]. By inserting the relativistic constant K_2 of eq. (1.21) into the mass equation, the absolute maximum mass (M_{Ch}) that can be supported by ideal electron degeneracy pressure is derived:

$$M_{Ch} = 4\pi \left(\frac{K_2}{\pi G}\right)^{\frac{3}{2}} \xi_1^2 |\theta'(\xi_1)| \qquad (3.17)$$

If a stellar degenerate core exceeds this limiting mass, the electron degeneracy pressure is insufficient to balance gravity, and the object will inevitably undergo further collapse.

3.3 Analysis of the Chandrasekhar Limit

In order to obtain a numerical value for the Chandrasekhar limit mass, it is necessary to solve the Lane-Emden equation for $n = 3$. Since this specific case lacks an analytical solution, a numerical integration was implemented in Python. The procedure relies on the *solve_ivp* function from the *SciPy* library, which employs a Runge-Kutta method to compute the dimensionless surface radius ξ_1 and $\theta'(\xi_1)$ with high precision.

To apply this numerical solver, the second-order Lane-Emden differential equation is decomposed into a system of two first-order ordinary differential equations:

$$\frac{dy_0}{d\xi} = y_1 \tag{3.18}$$

$$\frac{dy_1}{d\xi} = -y_0^3 - \frac{2}{\xi}y_1 \tag{3.19}$$

where $y_0 = \theta$ and $y_1 = d\theta/d\xi$.

To prevent numerical instabilities and complex outputs caused by rounding errors, a safeguard parameter `theta_safe` forces y_0 to remain non-negative during the process.

The stellar surface is identified by the condition $\theta = 0$. When it is met, the integration terminates, allowing the extraction of the exact values for ξ_1 and $\theta'(\xi_1)$.

Finally, to bypass the coordinate singularity at the center of the star ($\xi = 0$), the integration is initialized at $\xi_{start} = 10^{-4}$. The initial conditions at this point are analytically derived using a Taylor series expansion of $\theta(\xi)$ and $d\theta/d\xi$ around the origin.

The program gives the following values:

$$\xi_1 = 6.89685 \tag{3.20}$$

$$\theta'(\xi_1) = 0.04243 \tag{3.21}$$

$$\xi_1^2|\theta'(\xi_1)| = 2.01824 \tag{3.22}$$

These results were obtained considering $\mu_e = 2$, an approximation valid for helium and carbon-oxygen white dwarfs. By inserting the result (3.22) into equation (3.17), using the constant K_2 of eq. (1.21), the Chandrasekhar limit is obtained:

$$M_{ch} \approx 1.4559\mathrm{M}_\odot \tag{3.23}$$

This theoretical model predicts that white dwarfs with a mass greater than this limit cannot exist. Observational data, for the moment, confirm this assumption.

To see the Python code used for this analysis, see Appendix (A.1).

3.4 Analysis of the M-R relation

In this section, the mass-radius relationship obtained from the Lane-Emden equation for the case of non-relativistic electrons ($n = 3/2$) will be analyzed. The theoretical model thus obtained will be compared with experimental data to verify its validity and address its limitations.

To carry out this comparison, a numerical integration was implemented. The algorithm solves the Lane-Emden equation for $n = 1.5$.

At this point, thanks to the *NumPy* library, an array has been created with 100 central density values, equally spaced ranging from 10^5 g cm^{-3} up to 10^9 g cm^{-3}. Using eq. (3.9), eq. (3.13) and eq. (3.14), 100 fictitious WDs were created that follow the mass-radius relationship in the case of the polytropic with $n = 1.5$ and in this way it was possible to trace the curve shown as a solid blue line in Figure 3.2.

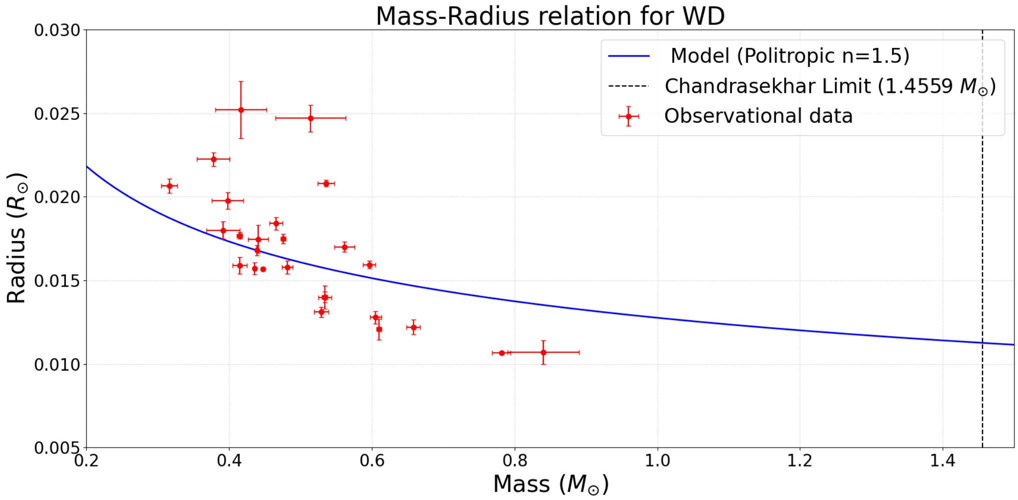

Figure 3.2: Theoretical mass-radius relation (solid blue line) and comparison with observational data (red circles). The Chandrasekar mass limit is marked with a vertical dashed line.

Object	g mag	P_{orb} (h)	T_{eff} (K)	Mass ($\mathrm{M}_\odot$)	Radius ($\mathrm{R}_\odot$)
CSS 080502	17.08	3.587	17 838 ± 482	0.4756 ± 0.0036	0.017 49 ± 0.000 28
CSS 09704	18.41	3.756	29 969 ± 679	0.4164 ± 0.0356	0.025 21 ± 0.001 70
CSS 21357	17.29	5.962	15 909 ± 285	0.6579 ± 0.0097	0.012 21 ± 0.000 46
CSS 40190	18.16	3.123	14 901 ± 731	0.4817 ± 0.0077	0.015 78 ± 0.000 39
CSS 41177A	17.27	2.784	22 497 ± 60	0.3780 ± 0.0230	0.022 24 ± 0.000 41
CSS 41177B	17.27	2.784	11 864 ± 281	0.3160 ± 0.0110	0.020 66 ± 0.000 42
GK Vir	16.81	8.264	50 000 ± 673	0.5618 ± 0.0142	0.017 00 ± 0.000 30
NN Ser	16.43	3.122	63 000 ± 3000	0.5354 ± 0.0117	0.020 80 ± 0.000 20
QS Vir	14.66	3.618	14 220 ± 350	0.7816 ± 0.0130	0.010 68 ± 0.000 07
RR Cae	14.57	7.289	7540 ± 175	0.4475 ± 0.0015	0.015 68 ± 0.000 09
SDSS J0024+1745	18.71	4.801	8272 ± 580	0.5340 ± 0.0090	0.013 98 ± 0.000 70
SDSS J0106−0014	18.14	2.040	13 957 ± 531	0.4406 ± 0.0144	0.017 47 ± 0.000 83
SDSS J0110+1326	16.53	7.984	24 569 ± 385	0.4656 ± 0.0091	0.018 40 ± 0.000 36
SDSS J0138−0016	18.84	1.746	3570 ± 100	0.5290 ± 0.0100	0.013 10 ± 0.000 30
SDSS J0314+0206	16.95	7.327	46 783 ± 7706	0.5964 ± 0.0088	0.015 94 ± 0.000 22
SDSS J0857+0342	17.95	1.562	37 400 ± 400	0.5140 ± 0.0490	0.024 70 ± 0.000 80
SDSS J1021+1744	19.51	3.369	10 644 ± 1721	0.5338 ± 0.0038	0.014 01 ± 0.000 32
SDSS J1028+0931	16.40	5.641	12 221 ± 765	0.4146 ± 0.0036	0.017 68 ± 0.000 20
SDSS J1123−1155	17.99	18.459	10 210 ± 87	0.6050 ± 0.0079	0.012 78 ± 0.000 37
SDSS J1210+3347	16.94	2.988	6000 ± 200	0.4150 ± 0.0100	0.015 90 ± 0.000 50
SDSS J1212−0123	16.77	8.061	17 707 ± 35	0.4393 ± 0.0022	0.016 80 ± 0.000 30
SDSS J1307+2156	18.25	5.192	8500 ± 500	0.6098 ± 0.0031	0.01207 ± 0.000 61
SDSS J1329+1230	17.26	1.943	12 491 ± 312	0.3916 ± 0.0234	0.018 00 ± 0.000 52
SDSS J2235+1428	18.59	3.467	20 837 ± 773	0.3977 ± 0.0220	0.019 75 ± 0.000 50
V471 Tau	10.04	12.508	34 500 ± 1000	0.8400 ± 0.0500	0.010 70 ± 0.000 70
WD 1333+005	17.41	2.927	7740 ± 73	0.4356 ± 0.0016	0.015 70 ± 0.000 36

Table 3.1: White dwarf mass–radius measurements obtained from eclipsing binaries. For more details, see Parsons' paper[6].

Regarding the experimental data, they are taken from [6] and all tabulated in Table 3.1. The data were measured independently of the model, therefore they can be used to test it.

It is clearly seen from Figure 3.2 that the polytropic model has great limitations. Even for less massive stars there are large discrepancies, while for increasing mass (density), relativistic effects become increasingly important and the model tends to over-estimate stellar radii.

To obtain a more accurate description of the reality, it is necessary to also take into account electrostatic effects, whose corrections give smaller radii and higher central densities compared to the model used.
The effect of neutronization (inverse β-decay) was also neglected. This has consequences on the adiabatic index, generating a maximum in the M-R ratio.

As density continues to increase, inverse beta decay forces electrons to combine with protons, forming a neutron-rich core. At this stage, the white dwarf equation of state breaks down completely, marking the transition to the realm of neutron stars.

The pycnonuclear reactions that occur inside white dwarfs have not been included in this theoretical model.

The biggest approximation, which generates the largest discrepancies with observational data, is the fact of having used a polytropic coefficient $n = 1.5$ for all central densities, thus treating all white dwarfs as non-relativistic, which is not true.

Chapter 4

Neutron Stars

Neutron stars represent the final evolutionary stage for stars with initial masses between 8 and 25 $M_\odot$. They are compact objects even more extreme than white dwarfs, providing a unique cosmic laboratory for studying the connections between nuclear physics, particle physics, and astrophysics. Indeed, neutron stars pack their mass into a radius on the order of 10 kilometers, reaching a mean density of the order of 10^{15} $\mathrm{g\,cm^{-3}}$, well above the nuclear saturation density ($\rho_{nuc} \approx 2.8 \times 10^{14}$ $\mathrm{g\,cm^{-3}}$). This extreme environment makes their analysis fundamentally important, although several theoretical issues regarding their internal equation of state remain unsolved.

The existence of neutron stars was first proposed in 1934 by Baade and Zwicky [7], who correctly hypothesized that they would consist of matter at exceedingly high densities. They also made the prescient suggestion that neutron stars would be formed in the aftermath of supernova explosions. However, the first theoretical models of the internal structure of these objects were performed by Oppenheimer and Volkoff in 1939 [8].

The discovery by Hewish and Bell in 1968 [9] of the first radio pulsar (the famous LGM-1) transformed neutron stars from mathematical abstractions into real astrophysical entities. A pulsar is a highly magnetized, rapidly rotating neutron star that emits beams of electromagnetic radiation from its magnetic poles. This radiation is primarily driven by synchrotron emission, produced as relativistic electrons are accelerated along the intense magnetic field lines. As the star spins, these beams sweep through space and can only be observed when they point directly toward Earth, creating regular pulses typically detected in the radio band. This physical mechanism, known as the "lighthouse effect", is responsible for the pulsed appearance of the source. Since then, neutron stars have increasingly become a major subject of study, leading to the development of new theoretical models.

In this chapter, the mass-radius relationship of neutron stars will be addressed. The analysis will begin with a simple polytropic model to demonstrate the limitations of a Newtonian gravity approach. Subsequently, the 1939 Oppenheimer-Volkoff limit will be derived by introducing the framework of General Relativity through the TOV equation. Finally, a more realistic modern model, such as the SLy (Skyrme-Lyon) equation of state, will be discussed to account for the effects of the strong nuclear force.

4.1 The Newtonian Approach

Although the effects of General Relativity can be neglected in modeling white dwarfs, applying a purely Newtonian approach to neutron stars leads to a departure from physical reality. This section will demonstrate that the use of the classical hydrostatic equations and the Lane-Emden formalism used in Chapter 3 yield inconsistent results when scaled to nuclear densities.

By executing the numerical integration developed in Section 3.3 and using the relativistic neutron gas constant from eq. (1.23), the following theoretical mass limit is obtained:

$$M_{lim} \approx 5.72\mathrm{M}_{\odot}. \tag{4.1}$$

It is an extremely high limit; in fact, neutron stars with such great mass have never been observed.

By integrating the Lane-Emden equation with $n = 3/2$ numerically (see the Python script in Appendix A.3), the mass-radius relation shown in Figure 4.1 is obtained.

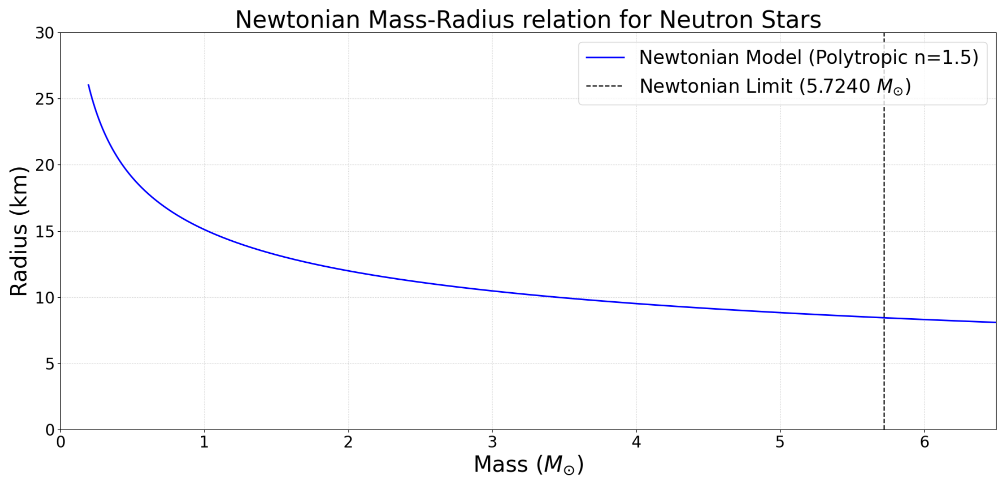

Figure 4.1: Theoretical mass-radius relation (solid blue line) using Newtonian gravity. The Newtonian mass limit is marked with a vertical dashed line

The Newtonian approximation neglects two crucial relativistic effects that dominate at these high densities. First, a neutron star generates an extreme curvature in spacetime, which is not described by Newtonian gravity, which assumes flat space.

Secondly, and most importantly, Newtonian physics completely ignores the mass-energy equivalence ($E = mc^2$). In the classical hydrostatic equilibrium equation, pressure only acts as an outward force resisting gravity. However, in the framework of General Relativity, all forms of energy contribute to the gravitational field. At the extreme conditions inside a neutron star, the kinetic energy of the degenerate neutrons is so immense that the internal pressure itself becomes a significant source of gravity.

This creates a vicious circle: the greater the pressure gradient required to contrast the gravitational contraction, the stronger the gravitational force generated by that same pressure. Since Newtonian gravity neglects this effect, it drastically overestimates the star's ability to support itself, leading to a much higher limiting mass. To solve this problem, the Newtonian hydrostatic equation must be replaced by the relativistic Tolman-Oppenheimer-Volkoff (TOV) equation, which will be addressed in the following section.

4.2 The TOV Approach

To construct a model that accurately reflects the extreme physics of neutron stars, it is necessary to introduce the framework of General Relativity.

The most general spherically symmetric metric can be written as:

$$ds^2 = -A(r,t)dt^2 + B(r,t)dr^2 + 2C(t,r)dtdr + D(r,t)d\Omega^2, \tag{4.2}$$

where $d\Omega^2 = d\theta^2 + \sin^2\theta d\phi^2$ is the angular coordinate, while t and r are the time and radial coordinates, respectively.

Through a series of mathematical transformations, it is possible to arrive at another formulation:

$$ds^2 = -e^{2\Phi}dt^2 + e^{2\lambda}dr^2 + r^2 d\Omega^2, \tag{4.3}$$

where Φ and λ are metric functions of t and r. For a star in stable hydrostatic equilibrium, these metric functions become independent of t.

In the case of a neutron star, extreme densities drive the matter into a highly degenerate state. Because thermal effects are negligible relative to the degeneracy pressure, the entropy contribution can be ignored. This allows for the use of an equation of state of the form:

$$P = P(\varepsilon), \tag{4.4}$$

where ε is the total energy density of the fluid.

By adopting geometrized units ($G = c = 1$) to simplify the notation, and defining a new metric function $m(r)$ by:

$$e^{2\lambda} \equiv \left(1 - \frac{2m}{r}\right)^{-1}, \tag{4.5}$$

Einstein's equations give:

$$\frac{dm}{dr} = 4\pi r^2 \varepsilon \tag{4.6}$$

$$\frac{dP}{dr} = -\frac{\varepsilon m}{r^2}\left(1 + \frac{P}{\varepsilon}\right)\left(1 + \frac{4\pi P r^3}{m}\right)\left(1 - \frac{2m}{r}\right)^{-1} \tag{4.7}$$

$$\frac{d\Phi}{dr} = -\frac{1}{\varepsilon}\frac{dP}{dr}\left(1 + \frac{P}{\varepsilon}\right)^{-1} \tag{4.8}$$

Equation (4.6) represents the mass continuity condition in General Relativity, where $m(r)$ is the total gravitational mass enclosed within the radius r.

Equation (4.7) is called "OV equation of hydrostatic equilibrium". Three relativistic correction factors emerge in the parentheses:

- The term $(1 + P/\varepsilon)$ represents a local relativistic effect: the internal pressure of a fluid element increases its effective inertial mass.
- The term $(1 + 4\pi P r^3/m)$ represents a global effect: it accounts for the fact that the pressure enclosed within the sphere of radius r contributes to the active gravitational field.
- The final term $(1-2m/r)^{-1}$ is a geometrical correction describing the extreme curvature of spacetime induced by the stellar mass.

In General Relativity, a stronger pressure gradient is required to counteract gravity compared to classical Newtonian physics. The Newtonian limit, expressed in eq. (3.4), is recovered by taking $P \ll \varepsilon$ and $GM/(rc^2) \ll 1$.

To solve the TOV equations, an explicit Equation of State $P(\varepsilon)$ is required. Following the historical approach of Oppenheimer and Volkoff [8], the neutron star is considered an ideal degenerate gas of neutrons.

The pressure P and the energy density ε can be expressed as a function of the dimensionless Fermi momentum x defined in eq. (1.16), replacing the electron mass m_e with the mass of the neutron:

$$P(x) = \frac{A}{3}\left[x(2x^2-3)\sqrt{x^2+1} + 3\sinh^{-1}(x)\right] \tag{4.9}$$

$$\varepsilon(x) = A\left[x(2x^2+1)\sqrt{x^2+1} - \sinh^{-1}(x)\right] \tag{4.10}$$

where $A \equiv m_n^4 c^5/(8\pi^2\hbar^3)$ is a constant derived from the phase-space integration of the Fermi-Dirac statistics for neutrons.

By numerically integrating the TOV equations coupled with this EoS (see the Python script in Appendix A.4), the impact of the relativistic corrections becomes evident.

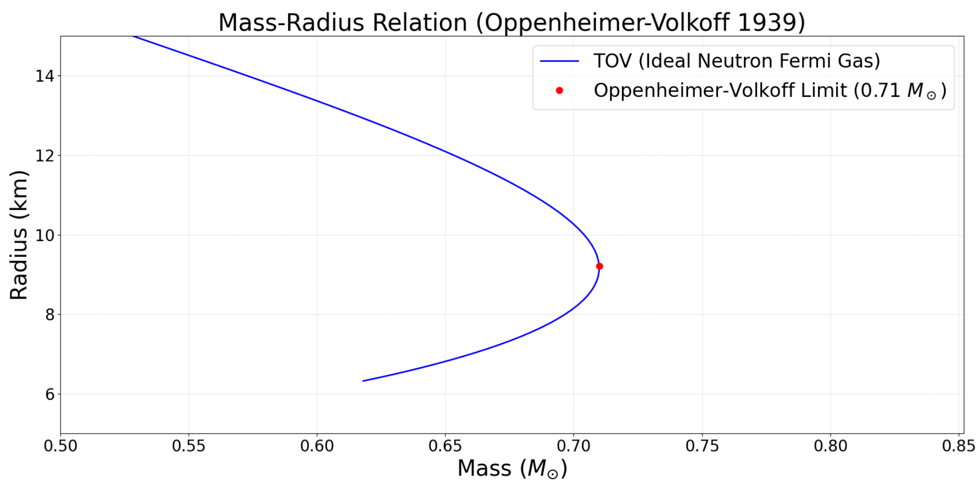

Figure 4.2: Relativistic Mass-Radius relation (solid blue line) calculated by Oppenheimer and Volkoff for an ideal neutron gas. The strong relativistic gravity causes the curve to peak at a lower mass limit (red dot).

As shown in Figure 4.2, the gravitational pull generated by the internal pressure forces the stellar structure to contract at a much lower mass compared to the Newtonian model.

There are three distinct regions of the graph to analyze:

- The Upper (Stable) Branch: Starting from the top left and moving along the curve toward the maximum mass, the central density increases. Along this branch, as mass is added, the radius decreases, which is the expected behavior for a degenerate object. These represent stable stellar configurations.
- The Critical Limit: The curve reaches a peak at $M_{OV} \approx 0.71$ $\mathrm{M}_{\odot}$. At this critical point, the core density and pressure are so extreme that the pressure itself becomes a primary source of gravitational collapse.
- The Lower (Unstable) Branch: Beyond the critical mass limit, mathematically increasing the central density yields configurations with lower mass and drastically smaller radii. In this branch, the derivative of the mass with respect to the central density becomes negative ($\frac{\partial M}{\partial \rho_c} < 0$). In astrophysics, this is the mathematical criterion for radial instability.

Numerically integrating the Oppenheimer-Volkoff model with the updated physical constants, a mass limit of $0.71 M_{\odot}$ and a radius of 9.21 km are obtained, consistent with the historical 1939 result of $\sim 0.7 M_{\odot}$. The discrepancy with modern observations, which have led to the discovery of neutron stars with masses of 2 $M_{\odot}$, shows that this approach also has limitations: the repulsion of the strong nuclear force has not been taken into account.

4.3 Modern Approach (SLy4)

The result of Oppenheimer and Volkoff is insufficient to describe the neutron star population observed in the modern era. The reason for this discrepancy lies in the assumption of an ideal, non-interacting gas. To resolve this limitation, modern models must incorporate the strong nuclear force. One of the most adopted models in astrophysics is the SLy (Skyrme-Lyon) Equation of State [10].

The SLy model introduces three fundamental physical improvements over the classical ideal gas approximation:

- Nucleon-Nucleon Interaction: At the extreme densities found in neutron star cores, nucleons are forced extremely close together. The SLy4 model uses a Skyrme effective interaction that accounts for the strong nuclear force [11]. Specifically, at very short distances, this potential becomes repulsive. This effect provides additional internal pressure.
- Beta-Equilibrium: Rather than assuming a pure neutron gas, the stellar interior is modeled as a mixture of neutrons, protons, electrons, and muons in thermodynamic β-equilibrium.

- Unified Description: The SLy EoS uses the exact same physical interaction to compute the properties of the solid outer crust and the dense liquid core, ensuring thermodynamic consistency across the entire star.

Due to its mathematical complexity, the SLy EoS is evaluated numerically. For this analysis, the official tabulated mass and radius data of the SLy4 EoS were extracted from the CompOSE (CompStar Online Supernovae Equations of State) database [12]. By processing these data through a Python script (see Appendix A.5), the mass-radius relation is obtained.

In Figure 4.3 it is clearly shown how the strong nuclear force allows the existence of neutron stars much more massive than the model of Oppenheimer and Volkoff.

The mass limit, in this case is

$$M_{SLy4} \approx 2.05\ M_\odot \tag{4.11}$$

with a corresponding radius of 10.00 km. This model successfully accounts for the existence of massive pulsars.

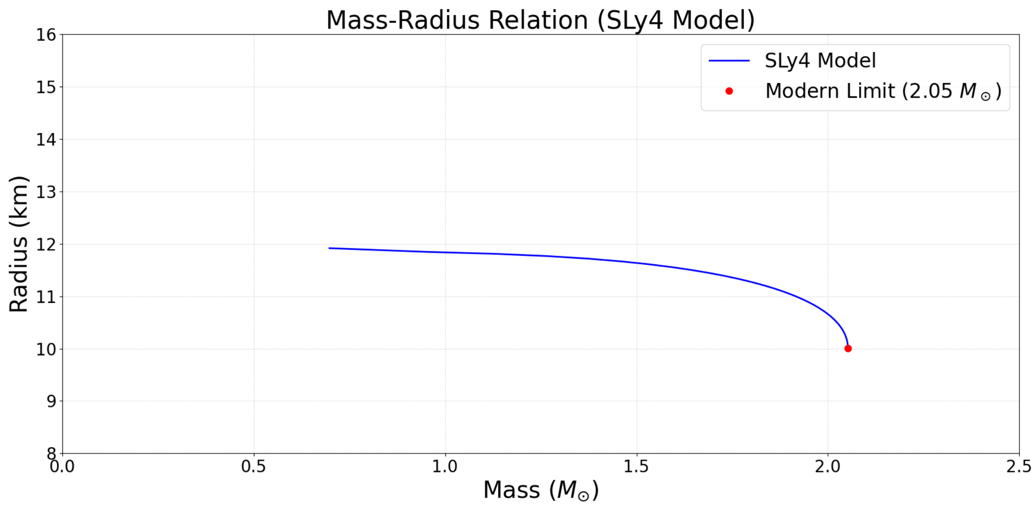

Figure 4.3: Mass-Radius relation (solid blue line) calculated with the SLy4 model. The repulsive strong nuclear force leads to a higher mass limit (red dot).

4.4 Comparison among charts

The comparison presented in Figure 4.4 aims to visually show the differences among the various approaches addressed in the previous sections, comparing them with observational data. Throughout this chapter, it has been shown how a classical approach, then a relativistic one, and finally a model that also takes nuclear interactions into account produce different predictions regarding the properties of neutron stars. By plotting these theoretical curves and comparing them with astrophysical measurements obtained from modern pulsar observations and gravitational wave events, summarized in Table 4.1, it becomes possible to assess the validity and limits of each mathematical model.

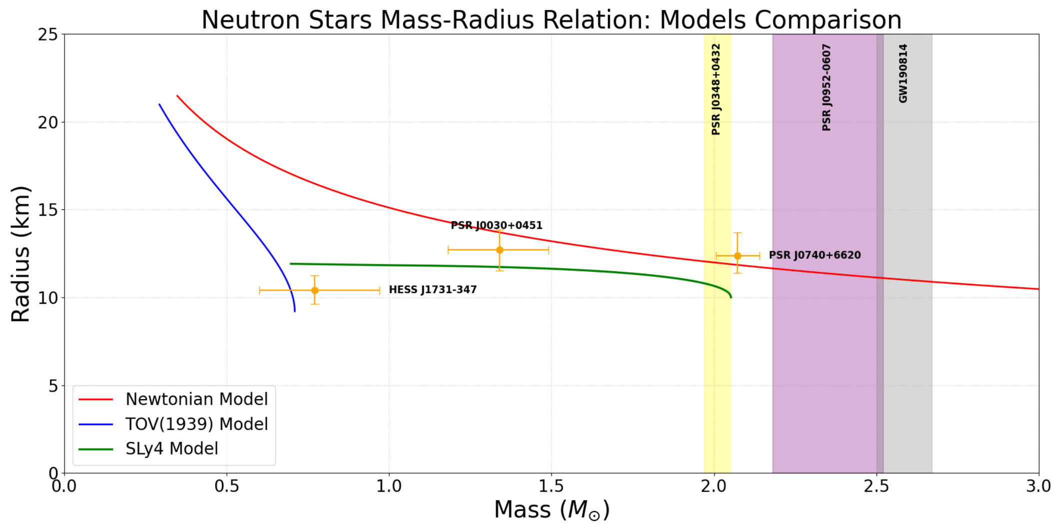

Figure 4.4: Mass-radius relationship of the three theoretical models (colored solid lines). Comparison with observational data (orange circles and colored regions).

Table 4.1: Observational data used for the Mass-Radius comparison. The unknown radii are denoted by dashes.

Object	**Mass ($M_\odot$)**	**Radius (km)**	**Ref.**
PSR J0030+0451	$1.34^{+0.15}_{-0.16}$	$12.71^{+1.14}_{-1.19}$	[13]
PSR J0740+6620	$2.072^{+0.067}_{-0.066}$	$12.39^{+1.30}_{-0.98}$	[14]
HESS J1731-347	$0.77^{+0.20}_{-0.17}$	$10.4^{+0.86}_{-0.78}$	[15]
PSR J0348+0432	2.01 ± 0.04	–	[16]
PSR J0952-0607	2.35 ± 0.17	–	[17]
GW190814	$2.50 - 2.67$	–	[18]

Firstly, the Newtonian ideal gas model (red line) is physically inadequate for several reasons. It completely ignores General Relativity, which is mandatory at such extreme densities. Furthermore, as a polytrope with $n = 1.5$, it predicts a mass-radius relation of $R \propto M^{-1/3}$. This inverse proportionality contradicts observational data, which instead show that neutron star radii remain remarkably constant, between 10 and 13 km across a wide range of masses.

Secondly, the ideal TOV model proposed by Oppenheimer and Volkoff (blue line) demonstrates what happens when General Relativity is applied without nuclear interactions. Because relativistic pressure contributes to gravity, the star collapses at a critically low mass of $M_{OV} \approx 0.71\ M_{\odot}$. The existence of much more massive objects like PSR J0740+6620 physically invalidates the Oppenheimer & Volkoff model, proving that a repulsive interaction is required to halt the collapse.

The SLy4 model (green line) resolves the most critical historical discrepancies. By incorporating the repulsive strong nuclear force at short distances, the EoS becomes stiffer, allowing the existence of massive pulsars and explaining the nearly constant radius trend.

However, a comparison with the most recent measurements reveals that the SLy4 approach is also not perfect. The observed radii for PSR J0030+0451 and PSR J0740+6620 are larger than the theoretical predictions of the SLy4 curve.

Moreover, the exact maximum mass of a neutron star remains an open question in modern astrophysics. Recent observations of the "black widow" pulsar PSR J0952-0607 and GW190814, a compact object that has not yet been identified as a black hole or neutron star, contradict the predictions of the SLy4 model. If objects significantly heavier than 2.05 $M_{\odot}$ are definitively confirmed as NS, it would imply that there are also other physical variables that have to be taken into consideration.

Understanding the maximum mass limit is essential because beyond that, no force can counteract gravity. The star is forced to collapse, becoming a Black Hole. These compact objects will be the focus of the next chapter.

Chapter 5

Black Holes

When a neutron star accretes matter and exceeds the mass limit, nothing can halt the collapse. The gravitational field near the object becomes stronger and stronger. Not even light can escape from the object to the outside world. The fate is the same for very massive stars, whose core mass is too large to form a NS.

A black hole is defined as a region of spacetime that cannot communicate with the external universe. The boundary of this region is called the event horizon.

Extrapolating Einstein's equations, they break down: a singularity develops. This problem could be solved with a quantum theory of gravitation; for this reason, black holes are extremely interesting compact objects to analyze.

Even though black holes do not emit light, they can be detected indirectly. First, gas falling into a black hole forms a hot accretion disk that emits strong radiation in X-ray and radio bands. Second, it is possible to study the motion of nearby stars and gas; their kinematics reveal the presence of a dark and compact point mass. Finally, gravitational waves from merging black holes offer a new way to study these extreme objects without using light. The first direct detection of these waves in 2015 is considered a major advancement that opened a new observational window on the universe.

While this thesis focuses on stellar-mass black holes from collapsing stars, they actually exist in many sizes. Supermassive Black Holes (SMBHs), millions or billions of times heavier than the Sun, sit at the center of most large galaxies. How they formed in the early universe is still a major mystery. Scientists are also searching for Intermediate-Mass Black Holes (IMBHs) to understand how these objects grow over time.

While realistic astrophysical black holes are expected to possess angular momentum and are accurately described by the Kerr metric, this chapter will not address rotating objects. This analysis will focus exclusively on the Schwarzschild solution.

Derived by Karl Schwarzschild in 1916, this metric provides the exact description of the gravitational field outside a spherical, uncharged, and non-rotating mass. Despite its simplicity, it contains all the essential physics required to understand both the event horizon and the spacetime geometry of a black hole.

5.1 The Schwarzschild Metric

An important result of Newtonian gravitation is that at any point outside a spherical mass distribution, the gravitational field depends only on the mass interior to that point. Moreover, even if the interior mass distribution is expanding or contracting while maintaining spherical symmetry, the field outside is constant in time. Recalling eq. (4.3), it simply means $\Phi = -M/r$.

This result is also true in general relativity, where it is known as Birkhoff's Theorem: any vacuum, spherically symmetric gravitational field is static. It is called the Schwarzschild metric:

$$ds^2 = -\left(1 - \frac{2M}{r}\right) dt^2 + \left(1 - \frac{2M}{r}\right)^{-1} dr^2 + r^2 d\theta^2 + r^2 \sin^2\theta d\phi^2, \tag{5.1}$$

expressed in geometrized units ($G = c = 1$). M is the mass of the source expressed in length units (i.e., $M = Gm/c^2$). The word "vacuum" denotes a region of spacetime where the gravitational effect of any matter present is negligible.

The Schwarzschild metric applies everywhere outside a spherical star, right up to its surface.

A static observer in this gravitational field is one who is at a fixed r, θ, ϕ coordinates. The proper time for such an observer is

$$d\tau = \sqrt{-ds^2} = \left(1 - \frac{2M}{r}\right)^{\frac{1}{2}} dt. \tag{5.2}$$

Looking at the equations above, it is clear that the metric breaks down at two critical points: at $r = 0$ (the intrinsic central singularity) and at $r = 2M$. The latter is known as the Schwarzschild radius and defines the event horizon, the surface of the black hole.

5.2 Nonsingularity of the Schwarzschild Radius

Looking at the metric in eq. (5.1) and the proper time in eq. (5.2), a singularity occurs at $r = 2M$. As the radial coordinate approaches this value, the coefficient of dt^2 goes to zero, while the coefficient of dr^2 becomes infinite.

From the perspective of a static observer positioned far away, an object falling towards the black hole would appear to slow down indefinitely due to extreme gravitational time dilation. The external observer would never actually see the object cross the radius $r = 2M$, as they would see it frozen and increasingly redshifted.

This led to the belief that $r = 2M$ was a physical boundary where spacetime itself ended. However, this is only a coordinate singularity. There is nothing locally special about this surface for an infalling observer.

To prove that the event horizon is not a physical singularity, one must compute an invariant quantity that does not depend on the choice of coordinates. In General Relativity, a standard measure of the curvature of spacetime is the Kretschmann scalar K, obtained by fully contracting the Riemann curvature tensor [19]. For a Schwarzschild black hole, the Kretschmann scalar is:

$$K = R^{\mu\nu\rho\sigma} R_{\mu\nu\rho\sigma} = \frac{48M^2}{r^6} \tag{5.3}$$

Evaluating this invariant scalar at the event horizon ($r = 2M$), the following value is obtained:

$$K(r = 2M) = \frac{48M^2}{(2M)^6} = \frac{3}{4M^4} \tag{5.4}$$

Since the result is a finite number, the intrinsic spacetime curvature at the event horizon is finite and smooth. Once an object crosses $r = 2M$, it must strike the singularity at $r = 0$; and once inside $r = 2M$, it cannot send signals back out to infinity. An observer does not notice anything significantly different in crossing from $r = 2M + \epsilon$ to $r = 2M - \epsilon$.

Restoring the physical constants G and c, the Schwarzschild radius is expressed as:

$$r_S = \frac{2Gm}{c^2}. \tag{5.5}$$

5.3 Singularities and Open Problems

If we evaluate the Kretschmann scalar in eq. (5.3) at the center of the black hole, taking the limit for $r \to 0$, we obtain:

$$\lim_{r \to 0} \frac{48M^2}{r^6} = +\infty. \tag{5.6}$$

Unlike the event horizon, which is a coordinate singularity, $r = 0$ represents a true physical singularity. As the radial coordinate approaches zero, the spacetime curvature diverges. Physically, this means infinite tidal forces, since the mass is concentrated in a region of infinite density.

It is important to note that the Schwarzschild metric describes a perfectly spherical, non-rotating vacuum spacetime. In reality, black holes are formed from the collapse of rotating stars, meaning they possess angular momentum. Such objects are described by the Kerr metric, where the central singularity is not a point, but rather a one-dimensional ring. However, regardless of the exact geometry, the presence of a singularity indicates a breakdown of the theory. When a physical parameter diverges to infinity, it usually means that the theory is incomplete and its limits of validity have been exceeded.

As matter collapses toward the singularity, its dimensions approach the Planck scale. Quantum effects are no longer negligible. Currently, the principles of Quantum Mechanics and General Relativity are mathematically incompatible. A unified theory of Quantum Gravity is required to describe such limiting regimes, but it remains one of the greatest open challenges in modern physics.

Studying black holes is therefore fundamental to the discovery of a unified theory capable of explaining physical reality even under extreme conditions.

Conclusions

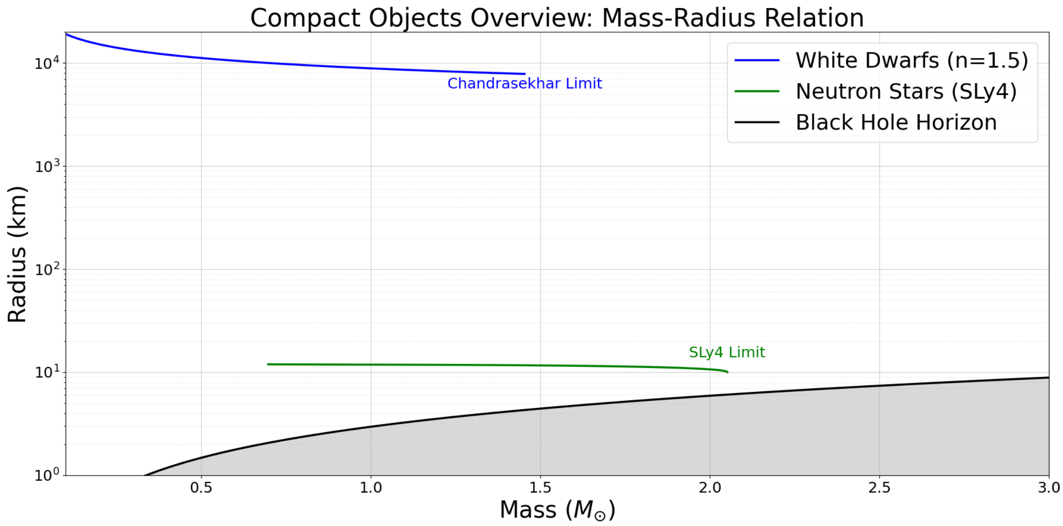

Figure C.1: Mass-radius relationship of the three classes of compact objects discussed in this thesis: white dwarfs (blue line), neutron stars (green line), black holes (black line).

This work investigated the macroscopic properties and the structure of compact objects, focusing on the critical mass-radius relationship. A key feature of this thesis was the computational approach: numerical solvers were implemented in Python to integrate the Lane-Emden equation and the Tolman-Oppenheimer-Volkoff equations. This allowed for the construction of theoretical models that were tested against modern observational data.

The data collected for White Dwarfs confirm the existence of the Chandrasekhar limit at $\sim 1.45 M_\odot$. However, comparing the theoretical $n = 1.5$ polytrope with data from eclipsing binaries clearly demonstrated the limitations of a purely non-relativistic model. It is necessary to include relativistic effects, inverse beta-decay, and electrostatic interactions for an accurate description of these objects.

The complexity of compact objects becomes most apparent in the study of neutron stars. The computational results showed that both the Newtonian approximation and the ideal relativistic Oppenheimer-Volkoff model fail to account for the observed masses of pulsars. The Newtonian approximation, while predicting an extremely high mass limit ($\sim 5.72 M_\odot$), is physically inadequate as it ignores spacetime curvature. On the other hand, the ideal relativistic Oppenheimer-Volkoff model applies General Relativity but fails in predicting a maximum mass of only $\sim 0.71 M_\odot$, which is far too low to account for the actual masses of observed pulsars. The inclusion of the strong nuclear force, modeled through the SLy4 Equation of State, provides the necessary repulsive pressure to halt the collapse, bringing the theoretical mass limit up to $\sim 2.05 M_\odot$. Yet, recent astronomical measurements of massive pulsars (such as PSR J0952-0607) and gravitational wave sources like GW190814 challenge even this advanced equation of state. The exact maximum mass of a neutron star remains one of the open questions in modern astrophysics.

Beyond this critical mass, gravity can no longer be stopped by quantum effects, leading to an inevitable collapse. The analysis of Black Holes via the Schwarzschild metric and the Kretschmann scalar demonstrated that, while the event horizon is a coordinate boundary, the central singularity represents a true physical breakdown of General Relativity. A unified theory of quantum gravity is necessary for a complete understanding of black holes.

Figure C.1 provides a visual summary of the results obtained in this thesis. By comparing the mass-radius relations, it highlights the differences in size and density among the three compact objects. The graph illustrates the transition from the electron degeneracy pressure of white dwarfs, to the complex nuclear interactions of neutron stars, up to the extreme spacetime curvature of black holes.

Appendix A

Python Code Snippets

A.1 Chandrasekhar_limit.py

This script computes the Chandrasekhar limiting mass by numerically solving the Lane-Emden equation for a relativistic degenerate electron gas ($n = 3$). Utilizing the *scipy.integrate.solve_ivp* function, the second-order differential equation is decomposed into a system of two first-order differential equations. The integration is initialized very close to the center using a Taylor expansion to bypass the coordinate singularity at the origin. It stops when the surface of the star is reached ($\theta = 0$) thanks to the *surface* function. Finally, the dimensionless results are scaled using the physical constants to output the theoretical maximum mass.

```python
import numpy as np
from scipy.integrate import solve_ivp

# system of two first-order differential equations
def lane_emden(xi, y, n):
    theta = y[0]
    dtheta = y[1]
    theta_safe = max(theta, 0.0)
    return [dtheta, -(theta_safe**n) - (2.0 / xi) * dtheta]

#stop event
def surface(xi, y, n):
    return y[0]
surface.terminal = True
surface.direction = -1

n = 3.0

#initial conditions (Taylor expansion)
xi_start = 1e-4

theta_start = 1.0 - (xi_start**2) / 6.0 + (n / 120.0) * (
   xi_start**4)
dtheta_start = -(xi_start) / 3.0 + (n / 30.0) * (xi_start**3)
```

```

#data resolution and extraction
solution = solve_ivp(
    fun=lane_emden, t_span=[xi_start, 20.0], y0=[theta_start,
        dtheta_start],
    args=(n,), events=surface, rtol=1e-10, atol=1e-12
)

xi_1_sol = solution.t_events[0][0]
dtheta_1_sol = abs(solution.y_events[0][0][1])

#Calculation of M_ch
G = 6.67430e-8
M_sun = 1.989e33
mu_e = 2.0

K_2 = 1.2435e15 / (mu_e**(4/3))

M_Ch_g = 4 * np.pi * ((K_2 / (np.pi * G))**(3/2)) * (xi_1_sol
   **2) * dtheta_1_sol

M_Ch_sun = M_Ch_g / M_sun

#Results
print("--- Results ---")
print(f"xi_1: {xi_1_sol:.5f}")
print(f"|dtheta/dxi|_xi1: {dtheta_1_sol:.5f}")
print(f"(xi_1^2*|theta'|): {(xi_1_sol**2)*dtheta_1_sol:.5f}\n
   ")

print("--- Chandrasekhar Limit ---")
print(f"M_Ch: {M_Ch_sun:.4f} Solar mass")
```

A.2 WD_Analysis.py

This code solves the Lane-Emden equation for the non-relativistic regime ($n = 1.5$). The script generates an array of central density values to construct the theoretical mass-radius curve for white dwarfs. It uses *matplotlib* for creating the chart and for comparing the model with the observational data from the eclipsing binaries.

```
import numpy as np
import matplotlib.pyplot as plt
from scipy.integrate import solve_ivp

# Lane-Emden Resolution

def lane_emden(xi, y, n):
    theta = y[0]
```

```
    dtheta = y[1]
    theta_safe = max(theta, 0.0)
    return [dtheta, -(theta_safe**n) - (2.0 / xi) * dtheta]

def surface(xi, y, n):
    return y[0]
surface.terminal = True
surface.direction = -1

def result(n):
    xi_start = 1e-4
    theta_start = 1.0 - (xi_start**2) / 6.0 + (n / 120.0) * (
       xi_start**4)
    dtheta_start = -(xi_start) / 3.0 + (n / 30.0) * (xi_start
       **3)

    solution = solve_ivp(
        fun=lane_emden, t_span=[xi_start, 20.0], y0=[
           theta_start, dtheta_start],
        args=(n,), events=surface, rtol=1e-8, atol=1e-10
    )
    return solution.t_events[0][0], abs(solution.y_events
       [0][0][1])

n = 1.5
xi_1_sol, dtheta_1_sol = result(n)

G = 6.67430e-8
M_sun = 1.989e33
R_sun = 6.957e10
mu_e = 2.0

K_1 = 1.0036e13 / (mu_e**(5/3))

#Generating an array of 100 WDs that follows the M-R relation
rho_c = np.logspace(5, 9, 100)

a = np.sqrt(((n + 1) * K_1 * rho_c**((1/n) - 1)) / (4 * np.pi
    * G))

radii_cm = a * xi_1_sol
masses_g = 4 * np.pi * (a**3) * rho_c * (xi_1_sol**2) *
   dtheta_1_sol

R_teo = radii_cm / R_sun
M_teo = masses_g / M_sun

# Observational data
# Format : (Mass M_sun , Radius R_sun , Error_M , Error_R ,
```

```
    Name)

wd_data = [
    (0.4756, 0.01749, 0.0036, 0.00028, "CSS 080502"),
    (0.4164, 0.02521, 0.0356, 0.00170, "CSS 09704"),
    (0.6579, 0.01221, 0.0097, 0.00046, "CSS 21357"),
    (0.4817, 0.01578, 0.0077, 0.00039, "CSS 40190"),
    (0.3780, 0.02224, 0.0230, 0.00041, "CSS 41177A"),
    (0.3160, 0.02066, 0.0110, 0.00042, "CSS 41177B"),
    (0.5618, 0.01700, 0.0142, 0.00030, "GK Vir"),
    (0.5354, 0.02080, 0.0117, 0.00020, "NN Ser"),
    (0.7816, 0.01068, 0.0130, 0.00007, "QS Vir"),
    (0.4475, 0.01568, 0.0015, 0.00009, "RR Cae"),
    (0.5340, 0.01398, 0.0090, 0.00070, "SDSS J0024+1745"),
    (0.4406, 0.01747, 0.0144, 0.00083, "SDSS J0106-0014"),
    (0.4656, 0.01840, 0.0091, 0.00036, "SDSS J0110+1326"),
    (0.5290, 0.01310, 0.0100, 0.00030, "SDSS J0138-0016"),
    (0.5964, 0.01594, 0.0088, 0.00022, "SDSS J0314+0206"),
    (0.5140, 0.02470, 0.0490, 0.00080, "SDSS J0857+0342"),
    (0.5338, 0.01401, 0.0038, 0.00032, "SDSS J1021+1744"),
    (0.4146, 0.01768, 0.0036, 0.00020, "SDSS J1028+0931"),
    (0.6050, 0.01278, 0.0079, 0.00037, "SDSS J1123-1155"),
    (0.4150, 0.01590, 0.0100, 0.00050, "SDSS J1210+3347"),
    (0.4393, 0.01680, 0.0022, 0.00030, "SDSS J1212-0123"),
    (0.6098, 0.01207, 0.0031, 0.00061, "SDSS J1307+2156"),
    (0.3916, 0.01800, 0.0234, 0.00052, "SDSS J1329+1230"),
    (0.3977, 0.01975, 0.0220, 0.00050, "SDSS J2235+1428"),
    (0.8400, 0.01070, 0.0500, 0.00070, "V471 Tau"),
    (0.4356, 0.01570, 0.0016, 0.00036, "WD 1333+005")
]

masses = [d[0] for d in wd_data]
radii = [d[1] for d in wd_data]
err_m = [d[2] for d in wd_data]
err_r = [d[3] for d in wd_data]
labels = [d[4] for d in wd_data]

#Plotting the graph

plt.figure(figsize=(9, 6))

plt.plot(M_teo, R_teo, 'b-', linewidth=2, label=" Model (
    Politropic n=1.5)")
plt.axvline(x=1.4559, color='k', linestyle='--', label="
    Chandrasekhar Limit (1.4559 $M_{\odot}$)")
plt.errorbar(masses, radii, xerr=err_m, yerr=err_r, fmt='o',
    color='red', capsize=3, label="Observational data")


```

```
plt.xlim(0.2, 1.5)
plt.ylim(0.005, 0.030)
plt.xlabel(r"Mass ($M_{\odot}$)", fontsize=28)
plt.ylabel(r"Radius ($R_{\odot}$)", fontsize=28)
plt.title("Mass-Radius relation for WD", fontsize=30)
plt.legend(loc='upper right', fontsize=24)
plt.grid(True, linestyle=':', alpha=0.7)
plt.tick_params(axis='both', which='major', labelsize=20)
plt.tight_layout()
plt.show()
```

A.3 NS_Newton.py

The following code is similar to the white dwarf scripts but utilizes the physical constants appropriate for a neutron gas. It solves the Lane-Emden equation for both $n = 3$ (to calculate the Newtonian mass limit) and $n = 1.5$ (to trace the mass-radius curve).

```
import numpy as np
import matplotlib.pyplot as plt
from scipy.integrate import solve_ivp

# Lane-Emden Resolution

def lane_emden(xi, y, n):
    theta = y[0]
    dtheta = y[1]
    theta_safe = max(theta, 0.0)
    return [dtheta, -(theta_safe**n) - (2.0 / xi) * dtheta]

def surface(xi, y, n):
    return y[0]
surface.terminal = True
surface.direction = -1

def result(n):
    xi_start = 1e-4
    theta_start = 1.0 - (xi_start**2) / 6.0 + (n / 120.0) * (
        xi_start**4)
    dtheta_start = -(xi_start) / 3.0 + (n / 30.0) * (xi_start
        **3)

    solution = solve_ivp(
        fun=lane_emden, t_span=[xi_start, 20.0], y0=[
            theta_start, dtheta_start],
        args=(n,), events=surface, rtol=1e-8, atol=1e-10
    )
```

```
    return solution.t_events[0][0], abs(solution.y_events
        [0][0][1])

n_NR = 1.5
xi_1_NR, dtheta_1_NR = result(n_NR)

n_UR = 3.0
xi_1_UR, dtheta_1_UR = result(n_UR)

G = 6.67430e-8
M_sun = 1.989e33

K_NR = 5.3802e9
K_UR = 1.2293e15

# Generating an array of 100 NSs that follows the M-R
   relation

rho_c = np.logspace(13.5, 17, 100)

# n=1.5

a = np.sqrt(((n_NR + 1) * K_NR * rho_c**((1/n_NR) - 1)) / (4
   * np.pi * G))
radii_cm = a * xi_1_NR
masses_g = 4 * np.pi * (a**3) * rho_c * (xi_1_NR**2) *
   dtheta_1_NR

R_teo_km = radii_cm / 1e5
M_teo_sun = masses_g / M_sun

#n=3

M_lim_g = 4 * np.pi * ((K_UR / (np.pi * G))**(1.5)) * (
   xi_1_UR**2) * dtheta_1_UR
M_lim_sun = M_lim_g / M_sun
print(f"M_lim_sun: {M_lim_sun:.4f} solar mass")

# Plotting the graph

plt.figure(figsize=(9, 6))
plt.plot(M_teo_sun, R_teo_km, 'b-', linewidth=2, label="
   Newtonian Model (Polytropic n=1.5)")
plt.axvline(x=M_lim_sun, color='k', linestyle='--', label=f"
   Newtonian Limit ({M_lim_sun:.4f} $M_{{\odot}}$)")
plt.xlim(0, 6.5)
plt.ylim(0, 30)

plt.xlabel(r"Mass ($M_{\odot}$)", fontsize=28)
```

```
plt.ylabel(r"Radius (km)", fontsize=28)
plt.title("Newtonian Mass-Radius relation for Neutron Stars", fontsize=30)
plt.legend(loc='upper right', fontsize=24)
plt.grid(True, linestyle=':', alpha=0.7)
plt.tick_params(axis='both', which='major', labelsize=20)
plt.tight_layout()

plt.show()
```

A.4 NS_TOV.py

This code solves the Tolman-Oppenheimer-Volkoff (TOV) equations for an ideal neutron gas. It uses *scipy.interpolate.interp1d* to map pressure to energy density and *solve_ivp* to integrate the equations from the core to the stellar surface. By iterating over different central pressures, the script constructs the relativistic mass-radius curve and identifies the Oppenheimer-Volkoff limit.

```
import numpy as np
import matplotlib.pyplot as plt
from scipy.integrate import solve_ivp
from scipy.interpolate import interp1d

G = 6.67430e-8
c = 2.99792458e10
M_sun = 1.989e33
m_n = 1.674927e-24
hbar = 1.0545718e-27

# EoS

A = (m_n**4 * c**5) / (8 * np.pi**2 * hbar**3)
x_arr = np.logspace(-3, 2, 10000)

P_arr = (A / 3) * (x_arr * (2 * x_arr**2 - 3) * np.sqrt(x_arr**2 + 1) + 3 * np.arcsinh(x_arr))
e_arr = A * (x_arr * (2 * x_arr**2 + 1) * np.sqrt(x_arr**2 + 1) - np.arcsinh(x_arr))

e_interp = interp1d(P_arr, e_arr, kind='cubic', fill_value="extrapolate")

# TOV Equations
def tov_equations(r, y):
    P, m = y

    if P <= 1e-10:
        return [0, 0]
```

```

    e = e_interp(P)
    rho = e / c**2

    term1 = 1.0 + P / e
    term2 = 1.0 + (4.0 * np.pi * r**3 * P) / (m * c**2)
    term3 = 1.0 - (2.0 * G * m) / (r * c**2)

    dP_dr = - (G * m * rho / r**2) * term1 * term2 / term3
    dm_dr = 4.0 * np.pi * r**2 * rho

    return [dP_dr, dm_dr]

def surface(r, y):
    return y[0] - 1e-5
surface.terminal = True
surface.direction = -1

masses = []
radii = []
P_c_values = np.logspace(33, 36.5, 100)

for P_c in P_c_values:
    r_start = 1e-5
    e_c = e_interp(P_c)
    rho_c = e_c / c**2
    m_start = (4.0 / 3.0) * np.pi * r_start**3 * rho_c

    solution = solve_ivp(
        fun=tov_equations,
        t_span=[r_start, 5e6],
        y0=[P_c, m_start],
        events=surface,
        rtol=1e-6,
        atol=1e-8
    )

    radii.append(solution.t[-1] / 1e5)
    masses.append(solution.y[1][-1] / M_sun)

# results and plot
max_mass = max(masses)
max_index = masses.index(max_mass)
corresponding_radius = radii[max_index]

print("\n--- HISTORICAL OPPENHEIMER-VOLKOFF LIMIT (1939) ---"
  )
print(f"Maximum Mass (M_OV): {max_mass:.4f} M_sun")
print(f"Corresponding Radius: {corresponding_radius:.4f} km\n
```

```
")

plt.figure(figsize=(9, 6))

plt.plot(masses, radii, 'b-', linewidth=2, label="TOV (Ideal Neutron Fermi Gas)")
plt.plot(max_mass, corresponding_radius, 'ro', markersize=8,
         label=f"Oppenheimer-Volkoff Limit ({max_mass:.2f} $M_\odot$)")

plt.xlim(0.5, max_mass * 1.2)
plt.ylim(5, 15)
plt.xlabel(r"Mass ($M_{\odot}$)", fontsize=28)
plt.ylabel(r"Radius (km)", fontsize=28)
plt.title("Mass-Radius Relation (Oppenheimer-Volkoff 1939)", fontsize=30)
plt.legend(loc='upper right', fontsize=24)
plt.grid(True, linestyle=':', alpha=0.7)
plt.tick_params(axis='both', which='major', labelsize=20)
plt.tight_layout()

plt.show()
```

A.5 NS_SLy4.py

This script processes realistic EoS data. Instead of solving differential equations from scratch, it reads tabulated mass and radius data for the SLy4 model obtained from the CompOSE database [12] using *numpy.loadtxt*. The script extracts the arrays, identifies the maximum stable mass and its corresponding radius, and plots the results.

```
import numpy as np
import matplotlib.pyplot as plt

#data reading and extraction
compose_data = np.loadtxt("eos/eos.mr", comments="#")

R_sly = compose_data[:, 0]
M_sly = compose_data[:, 1]

#maximum mass and radius
max_mass = np.max(M_sly)
max_index = np.argmax(M_sly)
corresponding_radius = R_sly[max_index]

#results and plot
print(f"Maximum Mass: {max_mass:.4f} M_sun")
```

```
print(f"Corresponding Radius: {corresponding_radius:.4f} km\n
    ")

plt.figure(figsize=(9, 6))
plt.plot(M_sly, R_sly, 'b-', linewidth=2, label="SLy4 Model")
plt.plot(max_mass, corresponding_radius, 'ro', markersize=8,
         label=f"Modern Limit ({max_mass:.2f} $M_\\odot$)")

plt.xlim(0, 2.5)
plt.ylim(8, 16)
plt.xlabel(r"Mass ($M_{\odot}$)", fontsize=28)
plt.ylabel(r"Radius (km)", fontsize=28)
plt.title("Mass-Radius Relation (SLy4 Model)", fontsize=30)
plt.legend(loc='upper right', fontsize=24)
plt.grid(True, linestyle=':', alpha=0.7)
plt.tick_params(axis='both', which='major', labelsize=20)
plt.tight_layout()

plt.show()
```

A.6 NS_comparison.py

This script combines the Newtonian, TOV, and SLy4 models into a single comparative graph. It uses *matplotlib* to plot these theoretical curves alongside modern observational data. Features like *errorbar* and *axvspan* are used to display confidence intervals, allowing a visual comparison between the theoretical models and the observed neutron stars.

```
import numpy as np
import matplotlib.pyplot as plt
from scipy.integrate import solve_ivp
from scipy.interpolate import interp1d

G = 6.67430e-8
c = 2.99792458e10
M_sun = 1.989e33
m_n = 1.674927e-24
hbar = 1.0545718e-27

# Newton
def lane_emden(xi, y, n):
    theta = y[0]
    dtheta = y[1]
    theta_safe = max(theta, 0.0)
    return [dtheta, -(theta_safe**n) - (2.0 / xi) * dtheta]

def surface(xi, y, n):
    return y[0]
```

```
surface.terminal = True
surface.direction = -1

def result(n):
    xi_start = 1e-4
    theta_start = 1.0 - (xi_start**2) / 6.0 + (n / 120.0) * (
        xi_start**4)
    dtheta_start = -(xi_start) / 3.0 + (n / 30.0) * (xi_start
        **3)

    solution = solve_ivp(
        fun=lane_emden, t_span=[xi_start, 20.0], y0=[
            theta_start, dtheta_start],
        args=(n,), events=surface, rtol=1e-8, atol=1e-10
    )
    return solution.t_events[0][0], abs(solution.y_events
        [0][0][1])

n_NR = 1.5
xi_1_NR, dtheta_1_NR = result(n_NR)

K_NR = 5.3802e9
rho_c_newt = np.logspace(14, 16.5, 100)
a = np.sqrt(((1.5 + 1) * K_NR * rho_c_newt**((1/1.5) - 1)) /
    (4 * np.pi * G))
R_newt = (a * xi_1_NR) / 1e5
M_newt = (4 * np.pi * (a**3) * rho_c_newt * (xi_1_NR**2) *
    dtheta_1_NR) / M_sun

# EoS
A = (m_n**4 * c**5) / (8 * np.pi**2 * hbar**3)
x_arr = np.logspace(-3, 2, 10000)

P_arr = (A / 3) * (x_arr * (2 * x_arr**2 - 3) * np.sqrt(x_arr
    **2 + 1) + 3 * np.arcsinh(x_arr))
e_arr = A * (x_arr * (2 * x_arr**2 + 1) * np.sqrt(x_arr**2 +
    1) - np.arcsinh(x_arr))

e_interp = interp1d(P_arr, e_arr, kind='cubic', fill_value="
    extrapolate")

# TOV
def tov_equations(r, y):
    P, m = y

    if P <= 1e-10:
        return [0, 0]

    e = e_interp(P)
```

```python
    rho = e / c**2

    term1 = 1.0 + P / e
    term2 = 1.0 + (4.0 * np.pi * r**3 * P) / (m * c**2)
    term3 = 1.0 - (2.0 * G * m) / (r * c**2)

    dP_dr = - (G * m * rho / r**2) * term1 * term2 / term3
    dm_dr = 4.0 * np.pi * r**2 * rho

    return [dP_dr, dm_dr]

def surface(r, y):
    return y[0] - 1e-5
surface.terminal = True
surface.direction = -1

M_tov = []
R_tov = []
P_c_values = np.logspace(33, 36.5, 100)

for P_c in P_c_values:
    r_start = 1e-5
    e_c = e_interp(P_c)
    rho_c = e_c / c**2
    m_start = (4.0 / 3.0) * np.pi * r_start**3 * rho_c

    solution = solve_ivp(
        fun=tov_equations,
        t_span=[r_start, 5e6],
        y0=[P_c, m_start],
        events=surface,
        rtol=1e-6,
        atol=1e-8
    )

    R_tov.append(solution.t[-1] / 1e5)
    M_tov.append(solution.y[1][-1] / M_sun)

max_mass = max(M_tov)
max_index = M_tov.index(max_mass)
corresponding_radius = R_tov[max_index]

# SLy4
compose_data = np.loadtxt("eos/eos.mr", comments="#")
R_sly = compose_data[:, 0]
M_sly = compose_data[:, 1]

#plot
plt.figure(figsize=(10, 7))
```

```
plt.plot(M_newt, R_newt, 'r-', linewidth=2, label="Newtonian Model")
plt.plot(M_tov, R_tov, 'b-', linewidth=2, label="TOV(1939) Model")
plt.plot(M_sly, R_sly, 'g-', linewidth=2.5, label="SLy4 Model")

# data
#Format: (Mass, Radius, Mass error, Radius error)
stars = {
    "PSR J0030+0451": [1.34, 12.71, [[0.16], [0.15]], [[1.19], [1.14]]],
    "PSR J0740+6620": [2.072, 12.39, [[0.066], [0.067]], [[0.98], [1.30]]],
    "HESS J1731-347": [0.77, 10.4, [[0.17], [0.20]], [[0.78], [0.86]]]
}

for name, data in stars.items():
    M = data[0]
    R = data[1]
    err_M = data[2]
    err_R = data[3]

    plt.errorbar(M, R, xerr=err_M, yerr=err_R,
                 fmt='o', color="orange", capsize=5, markersize=8)

    if name == "PSR J0030+0451":
        plt.text(M - 0.15, R + 1.35, name, fontsize=12, weight='bold', va='center')
    else:
        plt.text(M + err_M[1][0] + 0.03, R, name, fontsize=12, weight='bold', va='center')

plt.axvspan(2.01 - 0.04, 2.01 + 0.04, color='yellow', alpha=0.3)
plt.text(2.01, 24.5, "PSR J0348+0432", rotation=90, va='top', ha='center', fontsize=12, weight='bold')

plt.axvspan(2.35 - 0.17, 2.35 + 0.17, color='purple', alpha=0.3)
plt.text(2.35, 24.5, "PSR J0952-0607", rotation=90, va='top', ha='center', fontsize=12, weight='bold')

plt.axvspan(2.50, 2.67, color='grey', alpha=0.3)
plt.text(2.585, 24.5, "GW190814", rotation=90, va='top', ha='center', fontsize=12, weight='bold')
```

```

plt.xlim(0, 3)
plt.ylim(0, 25)
plt.xlabel(r"Mass ($M_{\odot}$)", fontsize=28)
plt.ylabel(r"Radius (km)", fontsize=28)
plt.title("Neutron Stars Mass-Radius Relation: Models
    Comparison", fontsize=30)
plt.legend(loc='lower left', fontsize=20)
plt.grid(True, linestyle=':', alpha=0.7)
plt.tick_params(axis='both', which='major', labelsize=20)
plt.tight_layout()

plt.show()
```

A.7 Compact_Objects.py

The final script generates the mass-radius comparison plot that summarizes the entire thesis. It reproduces the theoretical curves for white dwarfs ($n = 1.5$) and neutron stars (SLy4), and introduces the black hole event horizon by calculating the Schwarzschild radius across a linear array of masses. Because the spatial scales of these objects differ vastly, the script uses a logarithmic y-axis, providing a unified overview of the properties characterizing compact objects.

```
import numpy as np
import matplotlib.pyplot as plt
from scipy.integrate import solve_ivp

G = 6.67430e-8
c = 2.99792458e10
M_sun = 1.989e33
mu_e = 2.0

#WDs
def lane_emden(xi, y, n):
    theta = y[0]
    dtheta = y[1]
    theta_safe = max(theta, 0.0)
    return [dtheta, -(theta_safe**n) - (2.0 / xi) * dtheta]

def surface(xi, y, n):
    return y[0]
surface.terminal = True
surface.direction = -1

def result(n):
    xi_start = 1e-4
    theta_start = 1.0 - (xi_start**2) / 6.0 + (n / 120.0) * (
        xi_start**4)
```

```
    dtheta_start = -(xi_start) / 3.0 + (n / 30.0) * (xi_start
        **3)
    solution = solve_ivp(
        fun=lane_emden, t_span=[xi_start, 20.0], y0=[
            theta_start, dtheta_start],
        args=(n,), events=surface, rtol=1e-8, atol=1e-10
    )
    return solution.t_events[0][0], abs(solution.y_events
        [0][0][1])

n = 1.5
xi_1_sol, dtheta_1_sol = result(n)

K_1 = 1.0036e13 / (mu_e**(5/3))
rho_c = np.logspace(4, 9.5, 1000)

a = np.sqrt(((n + 1) * K_1 * rho_c**((1/n) - 1)) / (4 * np.pi
    * G))

R_wd_cm = a * xi_1_sol
M_wd_g = 4 * np.pi * (a**3) * rho_c * (xi_1_sol**2) *
    dtheta_1_sol

M_wd_teo = M_wd_g / M_sun
R_wd_teo = R_wd_cm / 1e5

valid_wd = M_wd_teo <= 1.4559
M_wd = M_wd_teo[valid_wd]
R_wd = R_wd_teo[valid_wd]

#NSs
compose_data = np.loadtxt("eos/eos.mr", comments="#")
R_ns = compose_data[:, 0]
M_ns = compose_data[:, 1]

#BHs
M_bh_array = np.linspace(0.1, 3.2, 200)
R_bh_cm = 2 * G * (M_bh_array * M_sun) / (c**2)
R_bh = R_bh_cm / 1e5

#plot
plt.figure(figsize=(11, 7))

plt.plot(M_wd, R_wd, 'b-', linewidth=2.5, label="White Dwarfs
    (n=1.5)")
plt.plot(M_ns, R_ns, 'g-', linewidth=2.5, label="Neutron
    Stars (SLy4)")
plt.plot(M_bh_array, R_bh, 'k-', linewidth=2.5, label="Black
    Hole Horizon")
```

```

plt.fill_between(M_bh_array, 0.1, R_bh, color='gray', alpha
    =0.3)

plt.text(1.4559, R_wd[-1] - 500, "Chandrasekhar Limit", color
    ='blue', fontsize=18, ha='center', va='top')
plt.text(M_ns[-1], R_ns[-1] + 3, "SLy4 Limit", color='green',
     fontsize=18, ha='center', va='bottom')

plt.yscale('log')

plt.xlim(0.1, 3.0)
plt.ylim(1, 20000)

plt.xlabel(r"Mass ($M_{\odot}$)", fontsize=28)
plt.ylabel(r"Radius (km)", fontsize=28)
plt.title("Compact Objects Overview: Mass-Radius Relation",
    fontsize=30)
plt.legend(loc='upper right', fontsize=26)

plt.grid(True, which="major", linestyle='-', alpha=0.6)
plt.grid(True, which="minor", linestyle=':', alpha=0.3)
plt.tick_params(axis='both', which='major', labelsize=18)

plt.tight_layout()
plt.show()
```

References

[1] Cesare Franchini. "Physics of matter". Lecture notes for the "Physics of matter" course taught by Prof. Cesare Franchini, Alma Mater Studiorum - Università di Bologna. 2025.

[2] Barbara Lanzoni. "Astrophysics". Lecture notes for the "Astrophysics" course taught by Prof. Barbara Lanzoni, Alma Mater Studiorum - Università di Bologna. 2025.

[3] Borb. *Overview of the triple-alpha process*. Licensed under CC BY-SA 3.0. [Online; accessed 12-June-2026]. 2006. URL: https://commons.wikimedia.org/w/index.php?curid=697609.

[4] S. Chandrasekhar. "The Maximum Mass of Ideal White Dwarfs". In: *The Astrophysical Journal* 74 (1931), p. 81. DOI: 10.1086/143324.

[5] S. Chandrasekhar. "The highly collapsed configurations of a stellar mass (Second paper)". In: *Monthly Notices of the Royal Astronomical Society* 95.3 (1935), pp. 207–225. DOI: 10.1093/mnras/95.3.207.

[6] S. G. Parsons et al. "Testing the white dwarf mass–radius relationship with eclipsing binaries". In: *Monthly Notices of the Royal Astronomical Society* 470.4 (June 2017), pp. 4473–4492. ISSN: 0035-8711. DOI: 10.1093/mnras/stx1522. eprint: https://academic.oup.com/mnras/article-pdf/470/4/4473/19179437/stx1522.pdf. URL: https://doi.org/10.1093/mnras/stx1522.

[7] Walter Baade and Fritz Zwicky. "Cosmic rays from super-novae". In: *Proceedings of the National Academy of Sciences* 20.5 (1934), pp. 259–263. DOI: 10.1073/pnas.20.5.259.

[8] J. R. Oppenheimer and G. M. Volkoff. "On Massive Neutron Cores". In: *Phys. Rev.* 55 (4 1939), pp. 374–381. DOI: 10.1103/PhysRev.55.374. URL: https://link.aps.org/doi/10.1103/PhysRev.55.374.

[9] Antony Hewish et al. "Observation of a rapidly pulsating radio source". In: *Nature* 217.5130 (1968), pp. 709–713. DOI: 10.1038/217709a0.

[10] F. Douchin and P. Haensel. "A unified equation of state of dense matter and neutron star structure". In: *Astronomy & Astrophysics* 380.1 (2001), pp. 151–167. DOI: 10.1051/0004-6361:20011402.

[11] E. Chabanat et al. "A Skyrme parametrization from subnuclear to neutron star densities". In: *Nuclear Physics A* 627.4 (1997), pp. 710–746. ISSN: 0375-9474. DOI: https://doi.org/10.1016/S0375-9474(97)00596-4. URL: https://www.sciencedirect.com/science/article/pii/S0375947497005964.

[12] A. Raduta and F. Gulminelli. *SLy4 Equation of State, CompOSE Database*. https://compose.obspm.fr/eos/134. Accessed: 2026-04-18, Unified EoS for cold neutron star matter. 2018.

[13] Thomas E. Riley et al. "A NICER View of PSR J0030+0451: Millisecond Pulsar Parameter Estimation". In: *The Astrophysical Journal Letters* 887.1 (2019), p. L21. DOI: 10.3847/2041-8213/ab481c.

[14] Thomas E. Riley et al. "A NICER View of the Massive Pulsar PSR J0740+6620 Informed by Radio Timing and XMM-Newton Spectroscopy". In: *The Astrophysical Journal Letters* 918.2 (2021), p. L27. DOI: 10.3847/2041-8213/ac0a81. URL: https://doi.org/10.3847/2041-8213/ac0a81.

[15] Victor Doroshenko et al. "A strangely light neutron star within a supernova remnant". In: *Nature Astronomy* 6 (2022), pp. 1444–1451. DOI: 10.1038/s41550-022-01800-1.

[16] John Antoniadis et al. "A Massive Pulsar in a Compact Relativistic Binary". In: *Science* 340.6131 (2013), p. 1233232. DOI: 10.1126/science.1233232.

[17] Roger W. Romani et al. "PSR J0952-0607: The Fastest and Heaviest Known Galactic Neutron Star". In: *The Astrophysical Journal Letters* 934.2 (2022), p. L17. DOI: 10.3847/2041-8213/ac8007.

[18] R. Abbott et al. "GW190814: Gravitational Waves from the Coalescence of a 23 Solar Mass Black Hole with a 2.6 Solar Mass Compact Object". In: *The Astrophysical Journal Letters* 896.2 (2020), p. L44. DOI: 10.3847/2041-8213/ab960f.

[19] Richard Conn Henry. "Kretschmann Scalar for a Kerr-Newman Black Hole". In: *The Astrophysical Journal* 535.1 (2000), p. 350. DOI: 10.1086/308819. URL: https://doi.org/10.1086/308819.

[20] Stuart L. Shapiro and Saul A. Teukolsky. *Black Holes, White Dwarfs, and Neutron Stars: The Physics of Compact Objects*. WILEY-VCH, 2004.

[21] Bernard Schutz. *A First Course in General Relativity*. 3rd ed. Cambridge University Press, 2022.

[22] A. Weigert R. Kippenhahn. *Stellar Structure and Evolution*. 1st ed. Springer-Verlag, 1990.

[23] Norman K. Glendenning. *Special and General Relativity: With Applications to White Dwarfs, Neutron Stars and Black Holes*. Springer, 2007.